Characteristics and consequences of H_2O undersaturation and low melt fertility in mountain belt interiors

Nicholas A. Lucas (nl423@cam.ac.uk)[1], Owen M. Weller (ow212@cam.ac.uk)[1], Marc R. St-Onge (marc.st-onge@nrcan-rncan.gc.ca)[2]

October 15, 2026

[1]Department of Earth Sciences, University of Cambridge, UK
[2]Geological Survey of Canada, Ottawa, Ontario, Canada

Peer review status: This is a non-peer-reviewed preprint submitted to EarthArXiv.

1 Abstract

Continental deformation and crustal magmatism in orogenic settings are fundamentally linked to fluid availability and melting processes. Critical rheological transitions occur at approximately 7% melt volume, whereby melt-film connectivity reduces rock strength by as much as c. 90%, and at 20%, marking an onset of solid-to-liquid behaviour. The Mesoproterozoic Grenville orogen in Canada provides an ideal orogenic locality to study such processes owing to its popular view as a 'large hot orogen' characterised by mid-crustal weakening; yet, large regions of the exposed orogenic mid-crust remain poorly understood in terms of melting history. Here we present new constraints on peak metamorphic P–T conditions, H_2O saturation and melt productivity across a 130-km across-strike transect perpendicular to the Sole Thrust in the western Grenville Province. While phase equilibrium modelling reveals relatively constant peak P–T conditions of ∼10 kbar and ∼750 °C across the transect, associated melt development was heterogeneous due to variable bulk rock chemistry and hydrous mineral content. Localised occurrences of aluminous pelite yielded ≥20 vol.% melt, but most regions record subsolidus conditions or generated low melt volumes, below the melt connectivity threshold, due to being fluid-undersaturated. Pervasive ductile flow and large-scale crustal weakening were therefore unlikely for this segment of the orogen. Even under conditions of H_2O saturation, temperatures exceeding 800 °C would have been required at 10 kbar to generate sufficient melt for bulk viscous flow (>20% melt).

2 Introduction

Exhumed mountain belts provide key records of metamorphic, magmatic and continental deformation processes at crustal levels generally inaccessible in active orogens (Brown, 1993, 2001; Weller et al., 2021). Some of the principles governing mountain building have been established through observations and models from ancient belts (e.g. Barrow, 1912; Argand, 1924; McKenzie, 1970; Molnar and Tapponnier, 1975; England and Thompson,

1984; Molnar and Lyon-Caen, 1988; Avouac, 2003; Brown, 1993; Kohn, 2014). However, there is much still to learn about the extent of fluid availability and melt generation in orogenic interiors, and their role in crustal differentiation, magmatism and deformation (e.g. Brown, 2001; Volante et al., 2025; Torvela and Kurhila, 2020; Kohn, Long, and Harrison, 2024; Whyte et al., 2021; Nicoli and Dyck, 2018; Austrheim, 1987; Ague, 2003). Crustal melt generation is viewed as being predominantly due to dehydration melting of hydrous minerals at mid- to lower-crustal depths (Clemens and Vielzeuf, 1987; Thompson, 1983; Tafur and Diener, 2020). In pelitic rocks, the onset of large melt production corresponds with vapour-absent muscovite breakdown at $\geq$650 °C and at biotite breakdown at $\geq$850 °C at typical mid-crustal pressures of $\geq$6 kbar (Spear, Kohn, and Cheney, 1999; White, Powell, and Holland, 2007). In rocks of quartzo-feldspathic composition (e.g. metagreywacke and tonalite), substantive melt is not produced until the breakdown of biotite at $\geq$800 °C (Johnson, White, and Powell, 2008; Palin et al., 2016). Mafic rocks produce smaller volumes of melt continuously over the temperature range relevant to most regional metamorphic terrains associated with the progressive breakdown of biotite and/or amphibole (Palin et al., 2016).

Temperatures between ~600 and 800 °Ccan yield a range of potential melt volumes depending on bulk rock chemistry and the availability of H_2O (Tafur and Diener, 2020; Clemens and Vielzeuf, 1987; Weinberg, Veveakis, and Regenauer-Lieb, 2015). Whereas free aqueous H_2O is unlikely to occur at these temperatures except where efficiently channelized (e.g. via shear zones), H_2O can be sourced from hydrous magmas to promote melting. A range of rheological behaviours can therefore occur, with up to 90% strength reductions at 7 vol.% melt corresponding to intergranular melt film connectivity (Rosenberg and Handy, 2005). Melt volumes above c. 20 vol.% correspond to a solid-to-liquid transition characterized by the suspension of crystalline material in liquid (Arzi, 1978; Rosenberg and Handy, 2005). Metamorphic terrains in which 20 vol.% or more melting is inferred at these moderate mid-crustal temperatures are uncommon (Weinberg, Veveakis, and Regenauer-Lieb, 2015) but have been reported (e.g. some leucogranites in the Himalayas; Le Fort et al., 1987). Composition and hydration state therefore play an important roles in determining the likely melt generation rates within mountain belts. For example, whether a fold-thrust belts is composed of hydrous, accreted passive margin material or previously-metamorphosed and dehydrated crust, could play a first-order control on mountain belt evolution.

In this study, we examine the varied control of bulk rock composition and H_2O saturation by constraining peak metamorphic conditions, H_2O content and melt productivity for a 130-km segment of the c. 1.1–1.0 Ga Grenville orogen in Canada (Fig. 1), owing to the widespread, continuous exposure of mixed lithologies with varying H_2O contents at mid-crustal depths (Rivers et al., 2012).

3 Geological setting

The Mesoproterozoic Grenville orogen in Canada is a globally important locality for research on continental deformation, owing to the widespread exposure of mid-crustal material (~30–40 km depth) (Dewey and Burke, 1973; Beaumont et al., 2006; Jamieson and Beaumont, 2013; Rivers, 2008; Rivers et al., 2012; Indares, 2020, 2024; Weller et al., 2021). Key characteristics include its extensive along-strike length (~2000 km), inferred double-thickness crust (~80 km) when the belt was active, high-temperature metamorphism (locally >800 °C) and long duration of deformation (c. 1090–985 Ma). The Grenville

orogen has been described as a 'large hot orogen', characterised by mid-crustal weakening and ductile, viscous flow (Jamieson et al., 2007; Rivers, 2011; Hynes and Rivers, 2010; Jamieson and Beaumont, 2011).

The Grenville orogen is predominantly exposed along the eastern margin of Canada, forming the type-locality of the orogen, and extends for approximately 2000 kilometres (red shade area, Fig. 1a). The Grenville orogenic event is considered to have initiated at c. 1190 Ma, with the main collisional event, which involved the amalgamation of the Amazonian and Laurentian cratons to form the supercontinent Rodinia, at 1090–985 Ma (Rivers, 1997; Rivers et al., 2012; Hynes and Rivers, 2010). Widespread pre-Grenvillian calc-alkaline intrusive suites across the Grenville in Canada imply that southeastern Laurentia was the site of arc magmatism and accretionary tectonics for >600 Myr (Rivers, 1997), leading up to the continent-continent collisional event.

The orogen is subdivided into two lithotectonic domains (Rivers et al., 1989): the 'Parautochthonous Belt', comprising Archean to Mesoproterozoic rocks of the Laurentian margin, and the structurally-overlying 'Allochthonous Belt', an imbricate of thrusted domains sourced from Laurentian crust and subordinate accreted island-arc terranes (Fig. 1b) (Rivers et al., 2012; Carr et al., 2000).

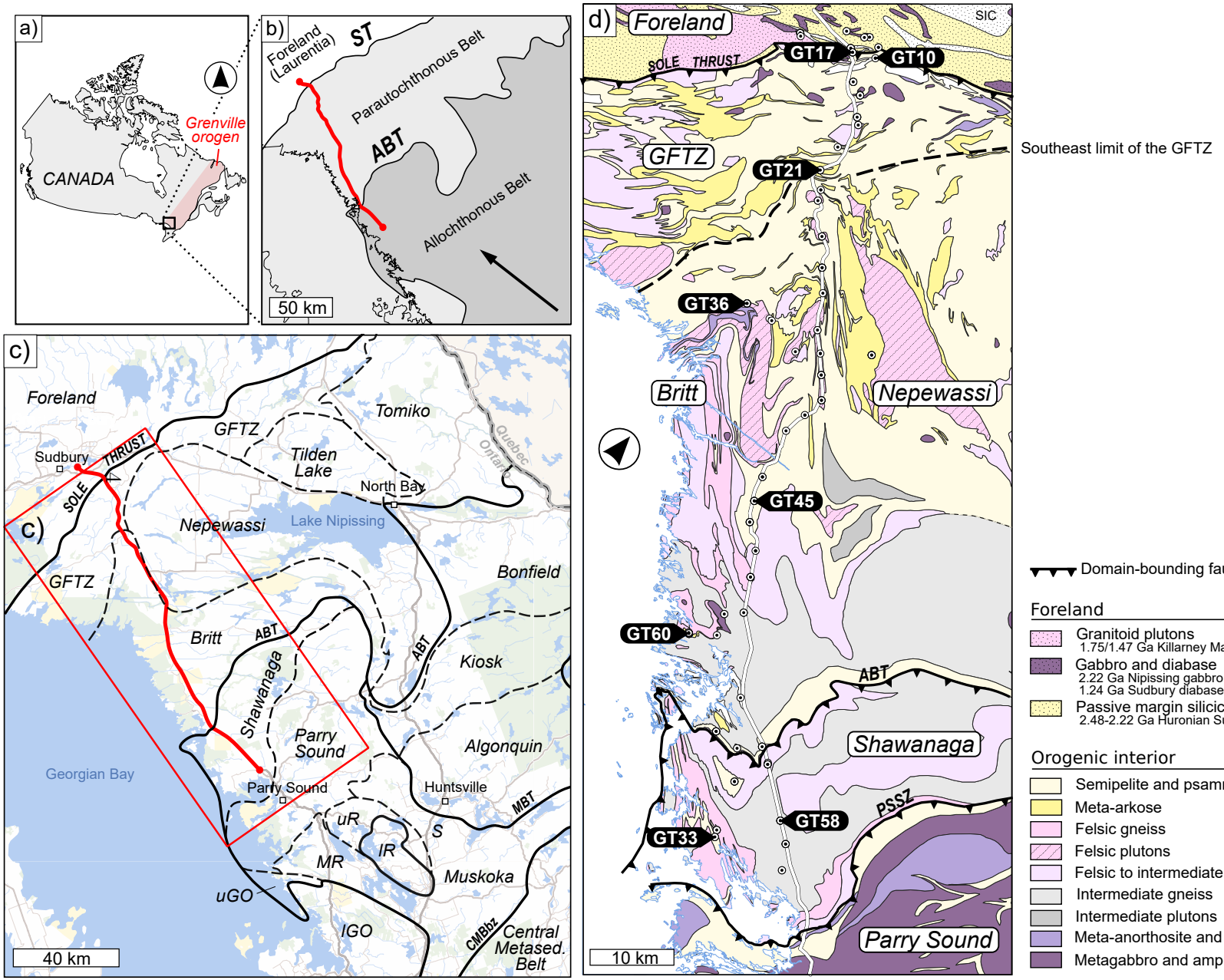

a)
CANADA
Grenville orogen
b)
Foreland (Laurentia)
ST
Parautochthonous Belt
ABT
Allochthonous Belt
50 km
c)
Foreland
GFTZ
Tomiko
Sudbury
THRUST
SOLE
Tilden Lake
North Bay
Quebec
Ontario
Nepewassi
Lake Nipissing
Bonfield
Britt
ABT
Shawanaga
Parry Sound
Kiosk
Algonquin
Georgian Bay
Parry Sound
Huntsville
MBT
uR
S
IR
MR
Muskoka
uGO
lGO
CMBbz
Central Metased. Belt
40 km
d)
Foreland
SIC
SOLE
THRUST
GT17
GT10
GFTZ
GT21
Southeast limit of the GFTZ
GT36
Britt
Nepewassi
GT45
GT60
ABT
Shawanaga
GT58
PSSZ
GT33
Parry Sound
10 km
Domain-bounding fault
Foreland
Granitoid plutons
1.75/1.47 Ga Killarney Mag. Belt
Gabbro and diabase
2.22 Ga Nipissing gabbro
1.24 Ga Sudbury diabase
Passive margin siliciclastics
2.48-2.22 Ga Huronian Supergroup
Orogenic interior
Semipelite and psammite
Meta-arkose
Felsic gneiss
Felsic plutons
Felsic to intermediate plutons
Intermediate gneiss
Intermediate plutons
Meta-anorthosite and -gabbro
Metagabbro and amphibolite

Figure 1: Location and geological maps of the studied transect adjacent to Georgian Bay in Ontario, Canada. (a) Simplified location map of Canada with the extent of the Grenville orogen highlighted in red. (b) Map of the main lithotectonic belts according to Rivers et al. (1989) in the western Grenville Province, in the region shown in (a). The red line denotes the study transect, which coincides with a major road (Highway 200/69). The black arrow indicates the approximate northwest direction of thrust propagation towards the foreland, perpendicular to the orogenic strike. The shoreline of Georgian Bay (lake) parallels the transect and is shown by black outline. (c) Land-use map annotated with geological domains (italicised text), modified from Culshaw et al. (2016). Abbreviations are as follows: GFTZ = Grenville Frontal Thrust Zone, ABT = Allochthon Boundary Thrust, CMBbz = Central Metasedimentary Belt Boundary Zone, MBT = Main Boundary Thrust. See Culshaw et al. (2016) for a full list of the domains. From northwest to southeast, the study transect (red line) traverses the foreland, GFTZ, Britt Domain and Shawanaga Domain. The red line is the road as shown in (b). (d) Updated geological map based on Culshaw et al. (2004), Davidson (1996), Davidson, Culshaw, and Nadeau (1982), and Ontario Geological Survey (2011). The eight study samples discussed in text are denoted by black labels, and Georgian Bay is coloured white with the coastline in blue.

3.1 Study area

In this study we focus on a 130-km across-strike transect in the western Grenville Province, adjacent to Georgian Bay in Ontario, Canada (red lines, Fig. 1b,c). This transect spans the orogenic foreland in the northwest and two structurally-overlying thrust sheets toward the southeast: the 'Britt Domain' and the 'Shawanaga Domain', respectively.

Samples were obtained along Highway 200/69 in Ontario (red line, Fig. 1b,c). From northwest to southeast, the main lithotectonic elements include: (1) the immediate footwall of the Sole Thrust; (2) the Sole Thrust and Grenville Frontal Thrust Zone (GFTZ); (3) the Britt Domain (part of the Parautochthonous Belt); and (4) the Shawanaga Domain (part of the Allochthonous Belt), with the Allochthon Boundary Thrust as its northwest boundary and the Parry Sound Shear Zone (PSSZ) as its southeast boundary (Fig. 1c,d). The term 'Sole Thrust' is used in this paper to designate the historic 'Grenville Front' (after Derry, 1950) based on seismic models that show it forms a basal decollement beween the deformed orogenic crust and the underthrusting relatively undeformed foreland (Green et al., 1988; White et al., 2000). The three domains in the hangingwall of the Sole Thrust are described below.

Rocks across the study region have previously been documented as migmatites or as exhibiting 'migmatite-like' textures due to the common occurrence of granitic segregations or layers that are coarser-grained than the surrounding rock (Lumbers, 1975; Davidson, Culshaw, and Nadeau, 1982; Davidson, 1986; Jamieson et al., 1992; Jamieson, Culshaw, and Corrigan, 1995; Corrigan, Culshaw, and Mortensen, 1994; Wodicka, Ketchum, and Indares, 2000). Outcrop-based estimates for melt proportions across the GFTZ and northwest Britt Domain are between 5 and 20% (Ontario Geological Survey, 1974; Easton and Murphy, 2002).

Sole Thrust and Grenville Frontal Thrust Zone (GFTZ)
The Sole Thrust forms the northwest boundary of the Grenville Front Tectonic Zone ('GFTZ', after Wynne-Ewards, 1972) and is present along the full length of the exposed orogen (Rivers et al., 1989). The GFTZ forms a region up to 30 km wide of anastomosing

southeast-dipping shear zones that accommodated northwestward thrusting of the orogenic front relative to the adjacent foreland between c. 1000 and 990 Ma (e.g. Davidson and Bethune, 1988; Jamieson, Culshaw, and Corrigan, 1995; Krogh, 1994; Corfu and Easton, 2001; Bethune, 1997). Meta-siliciclastic and granitoid gneiss are the dominant lithologies. The protoliths include c. 1750 Ma and c. 1470 Ma plutonic rocks and 2480–2220 Ma metasedimentary sequences as found in the proximal orogenic foreland (Davidson, 1986; Bennett, Dressler, and Robertson, 1991). The GFTZ is delimited at its southeastern boundary with the Britt Domain by a progressive structural transition to shallowly southeast-plunging folds (roughly denoted by the dashed line in Fig. 1d; Davidson and Bethune, 1988; Jamieson, Culshaw, and Corrigan, 1995; Pryer, 1985). Reported metamorphic conditions for the GFTZ mainly range from 6 to 10 kbar and 660 to 750 °C (Anovitz and Essene, 1990; Davidson, Carmichael, and Pattison, 1990; Bethune and Davidson, 1997; Jamieson, Culshaw, and Corrigan, 1995; Corfu and Easton, 2001). Isograds vary over a 10 km distance southeast from the Sole Thrust from staurolite grade, to kyanite and sillimanite-K-feldspar-melt grade, indicating that metamorphic conditions locally increase towards the hinterland (Anovitz and Essene, 1990; Murphy, 1999; Kwak, 1971).

Britt Domain

The Britt Domain (Fig. 1d) comprises a thrust sheet with an across-strike width of ∼100 km. The main documented lithologies include 1750–1650 Ma and 1460–1430 Ma gneissic granitoid bodies and sheets, surrounded by layered psammite and meta-arkose gneiss (Lumbers, 1975; Corrigan, Culshaw, and Mortensen, 1994; Davidson, Culshaw, and Nadeau, 1982; Culshaw et al., 1988). These units define map-scale transverse folds southeast of the GFTZ (Fig. 1d). Plutonic rocks are compositionally varied—including granite to syenite (*sensu stricto*; pink unit in Fig. 1d), granodiorite to tonalite (light and dark grey), anorthosite (light purple) and gabbro (dark purple). The boundary between the Britt Domain and the 'Nepewassi domain' (to the northeast, marginal to the study transect; Fig. 1c,d) is defined by a transition from Paleoproterozoic to Archean Nd and Hf depleted-mantle model ages from zircon and the appearance of Archean orthogneiss (Slagstad et al., 2024), consistent with a shift in crustal source, from juvenille crust to reworked Archean crust at the time of Paleo- to Mesoproterozoic magmatism. To the southeast is the Allochthon Boundary Thrust (ABT), which separates the Britt Domain from the overlying Shawanaga Domain.

Reported metamorphic conditions range widely from 4 to 15 kbar and 500 to 870 °C (Anovitz and Essene, 1990; Tuccillo et al., 1992; Ketchum et al., 1994; Jamieson, Culshaw, and Corrigan, 1995; Chapman, 2017). The spread of these data has primarily been attributed to varied degrees of retrograde re-equilibration. Peak metamorphic conditions occurred in the kyanite field based on the abundance of this aluminosilicate across the Britt Domain (Tuccillo et al., 1992; Ketchum et al., 1994; Lumbers, 1975).

Shawanaga Domain and bounding shear zones (ABT, PSSZ)

The Shawanaga Domain is bound across strike by major southeast-dipping shear zones with down-dip lineations: the ABT to the northwest and the Parry Sound Shear Zone (PSSZ) to the southeast (Fig. 1d). The ABT is a 3 km-wide, sinuous shear zone that accommodated thrust emplacement of the Shawanaga Domain onto the Laurentian margin from 1091±6 Ma (Slagstad et al., 2004), followed by normal-sense motion active at 1019±4 Ma until 988±2 Ma (Ketchum et al., 1998). The PSSZ forms a ∼1 km wide shear zone that initiated as a thrust zone at 1121±5 Ma (Van Breemen et al., 1986) and is thought to have accommodated normal-sense motion contemporaneously with the ABT (Wodicka, Ketchum, and Indares, 2000; Culshaw, Gerbi, and Marsh, 2010).

The Shawanaga Domain has been described as a high-grade, migmatite-bearing thrust sheet comprising 1660–1640 Ma and 1480–1430 Ma metaplutonic gneiss, which appear in the map (Fig. 1d) as folded felsic plutonic sheets (pink and light purple units) and more volumetrically dominant intermediate gneiss (grey unit) (Slagstad et al., 2024, 2004). Semipelite and psammite (light yellow unit) are intercalated with metavolcanic rocks, and collectively form minor constituents in the thrust sheet. In general, the meta-igneous rocks are more intermediate in composition than those of the Britt Domain (Davidson, Culshaw, and Nadeau, 1982), and the metasedimentary-metavolcanic units are distinguished by their continental rift geochemistry (Culshaw and Dostal, 1997) and c. 1260 Ma detrital zircon signatures (Culshaw et al., 2013). Thus, although metaplutonic rocks suggest a linkage in magmatic history with the Britt Domain, the metasedimentary-metavolcanic units are correlated with c. 1290–1220 Ma volcanism in accreted arc terranes located >100 km to the southeast in present-day coordinates (i.e. in the Central Metasedimentary Belt, Fig. 1c; Carr et al., 2000).

Reported metamorphic conditions range from 4 to 11 kbar and 500 to 850 °C (Ketchum et al., 1994; Anovitz and Essene, 1990; Tuccillo et al., 1992; Wodicka, Ketchum, and Indares, 2000). Based on microstructural observations, these conditions encompass early high-grade metamorphism, partial melting and penetrative deformation at 1080–1050 Ma (Wodicka, Ketchum, and Indares, 2000; Ketchum et al., 1998), and static greenschist-grade re-equilibration at 970–960 Ma (Ketchum et al., 1998; Wodicka, Ketchum, and Indares, 2000). Occurrences of anhedral kyanite and overgrowths of sillimanite are consistent with this domain having undergone decompression and/or heating from kyanite- to sillimanite-grade metamorphic conditions (Tuccillo et al., 1992).

4 Petrography, mineral chemistry and pseudosection analysis

Fifty-six ∼equally-spaced hand samples were selected for thin section study. Eight of these samples (black labels, Fig. 1d) were identified as being most suitable for accurate P–T determination whilst capturing a range of mafic to intermediate and pelitic bulk compositions. Petrographic observations, mineral composition data and pseudosection analyses are presented below for each sample in turn, which are presented in order of increasing distance from the Sole Thrust (Fig. 1d). Interpreted equilibrium assemblages are summarised in Table S2.

4.1 Methods

Major element mineral analyses were acquired using a Cameca SX-100 electron probe micro-analyser (EPMA) and a JEOL JXA-iHP200F Field Emission EPMA, both at the University of Cambridge. Biotite formulae were calculated using the method of Li et al. (2020). Mineral formulae were calculated using the program AX (version Oct-2019; Holland (2009)). Mineral abbreviations follow Whitney and Evans (2010). Mineral chemistry data are provided in the Supplement.

Phase equilibrium modelling was performed using Theriak-Domino (version 11-Mar-2020; Capitani and Petrakakis, 2010) with dataset ds62 (Holland and Powell, 2011). The Na_2O-CaO-K_2O-FeO-MgO-Al_2O_3-SiO_2-H_2O-TiO_2-O (NCKFMASHTO) model system was used for mafic samples, with MnO additionally considered for pelitic samples, using the following activity-composition models: garnet, orthopyroxene, biotite, ilmenite-hematite,

magnetite-spinel and melt (White et al., 2014); augitic clinopyroxene and melt (Green et al., 2016); clino-amphibole (Green et al., 2016); feldspar (Baldwin et al., 2005); epidote (Holland and Powell, 2011); and muscovite (Coggon and Holland, 2002; White et al., 2014). Pure phases included the aluminosilicates, albite, coesite, H_2O, lawsonite, quartz, rutile, titanite and zoisite. Hornblende-plagioclase thermometry was additionally conducted using the calibration of Holland and Blundy (1994) (as updated in Molina et al., 2015). All samples contain quartz, hence the edenite-tremolite thermometer was employed.

4.2 Garnet-epidote psammite GT17 (Sole Thrust)

Sample GT17 was collected from an outcrop comprising mylonitic psammite located in the immediate hanging-wall of the Sole Thrust (Fig. 1d). Sample GT17 comprises feldspar porphyroclasts set in a fine-grained quartzofeldspathic matrix (<50 μm) (Fig. 2a). The analysed thin section contains: quartz (38 vol.%), K-feldspar (29 vol.%), plagioclase (21 vol.%), biotite (9 vol.%), epidote (2 vol.%), apatite (1 vol.%) and accessory (<1 vol.%) titanite, garnet, zircon, pyrrhotite, muscovite and monazite.

Quartz is disseminated throughout the matrix and in places forms discrete layers that likely represent quartz veins in the protolith (Fig. 2a). K-feldspar and plagioclase occur in a range of grain sizes, forming up to ~500 μm-sized augen porphyroclasts. K-feldspar augen are commonly embayed by fine-grained plagioclase (Fig. 2a), but the reverse is also observed (Fig. 2b). Plagioclase is dominantly albite in composition (X_{An} = Ca/(Ca + Na + K) = ~0.09), but oligoclase core compositions are common, with a maximum observed X_{An} of 0.19 (Fig. 2b). Both feldspars are observed in contact with the matrix phases. Biotite (X_{Mg} = 0.11-0.13) forms subhedral to anhedral laths up to ~20 μm across. Garnet occurs as anhedral grains up to ~700 μm in diameter, commonly rimmed by anhedral quartz, and wrapped by matrix biotite. Garnet grain interiors exhibit uniform compositions ($Alm_{63}Grs_{23}Sps_{14}Prp_1$), with more Fe-poor and Ca-rich outer rims. Epidote-group minerals form subhedral to anhedral porphyroblasts ~300 μm across, overgrowing the matrix and biotite foliation. Their composition is allanite in the cores and epidote in the mantles (pistacite content = $\frac{Fe^{3+}}{Fe^{3+}+Al}$ = 0.23-0.25). Titanite forms anhedral grains. Accessory muscovite overgrows feldspar porphyroclasts and is considered late.

Quartz, K-feldspar, oligoclase, albite, biotite, epidote, titanite and garnet are interpreted as an equilibrium assemblage based on their shared grain boundaries. The co-occurrence of albite and oligoclase is consistent with the sample having equilibrated at the greenschist-amphibolite transition (Maruyama, Liou, and Suzuki, 1982; Cooper, 1972; Bégin, 1992). The presence of (lower temperature) albite rims surrounding (higher temperature) oligoclase cores suggests that the preserved conditions were attained during retrograde metamorphism, at temperatures corresponding to the peristerite gap (less than ~450-600 °C; Maruyama, Liou, and Suzuki, 1982).

A P–T pseudosection (Fig. 3a) constructed for sample GT17 shows that both the identified equilibrium assemblage (quartz, K-feldspar, oligoclase, albite, biotite, epidote, titanite and garnet) and inferred higher-temperature assemblage (all phases minus albite) are present across a P–T range of up to 9 kbar and 635 °C, separated by albite-out. To higher temperatures epidote is lost from the assemblage. The albite-stable field is bound at lower T/higher P by ilmenite or muscovite joining the assemblage (i.e. markers '4' and '2', respectively; Fig. 3a). Magnetite is also present in these model fields but was not observed in the sample; a T–$X(Fe^{3+})$ pseudosection in Supplementary Fig. S2a shows that a magnetite-free field appears between $X(Fe^{3+})$ = 0 and ~0.05, across which the

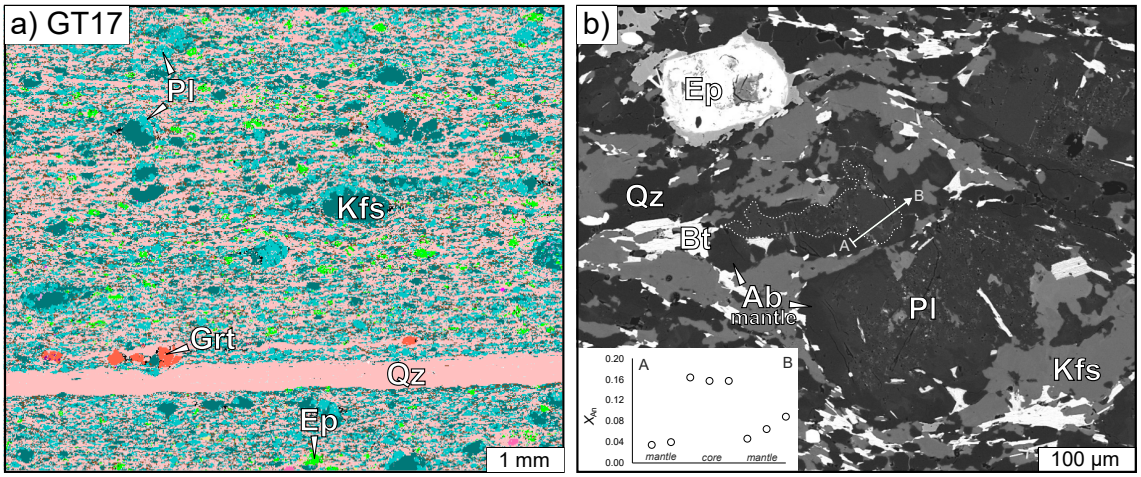


Figure 2: Sample GT17 petrography. (a) QEMSCAN phase map. (b) Back-scattered electron image showing plagioclase porphyroclasts surrounded by K-feldspar. The white dotted line divides the oligoclase core and albite rim of a plagioclase grain. Compositions along a transect of this grain are shown in the inset plot.

muscovite and epidote stability boundaries vary by ∼30 °C. Contours for X_{An} are displayed on Fig. 3a and match only compositions within the cores of oligoclase grains (up to X_{An} = 0.19). The contouring refines the P–T range to 6.8–8.5 kbar and 575–610 °C. These conditions straddle the albite-absent and -stable fields, consistent with the petrographic interpretation that this sample equilibrated close to this transition.

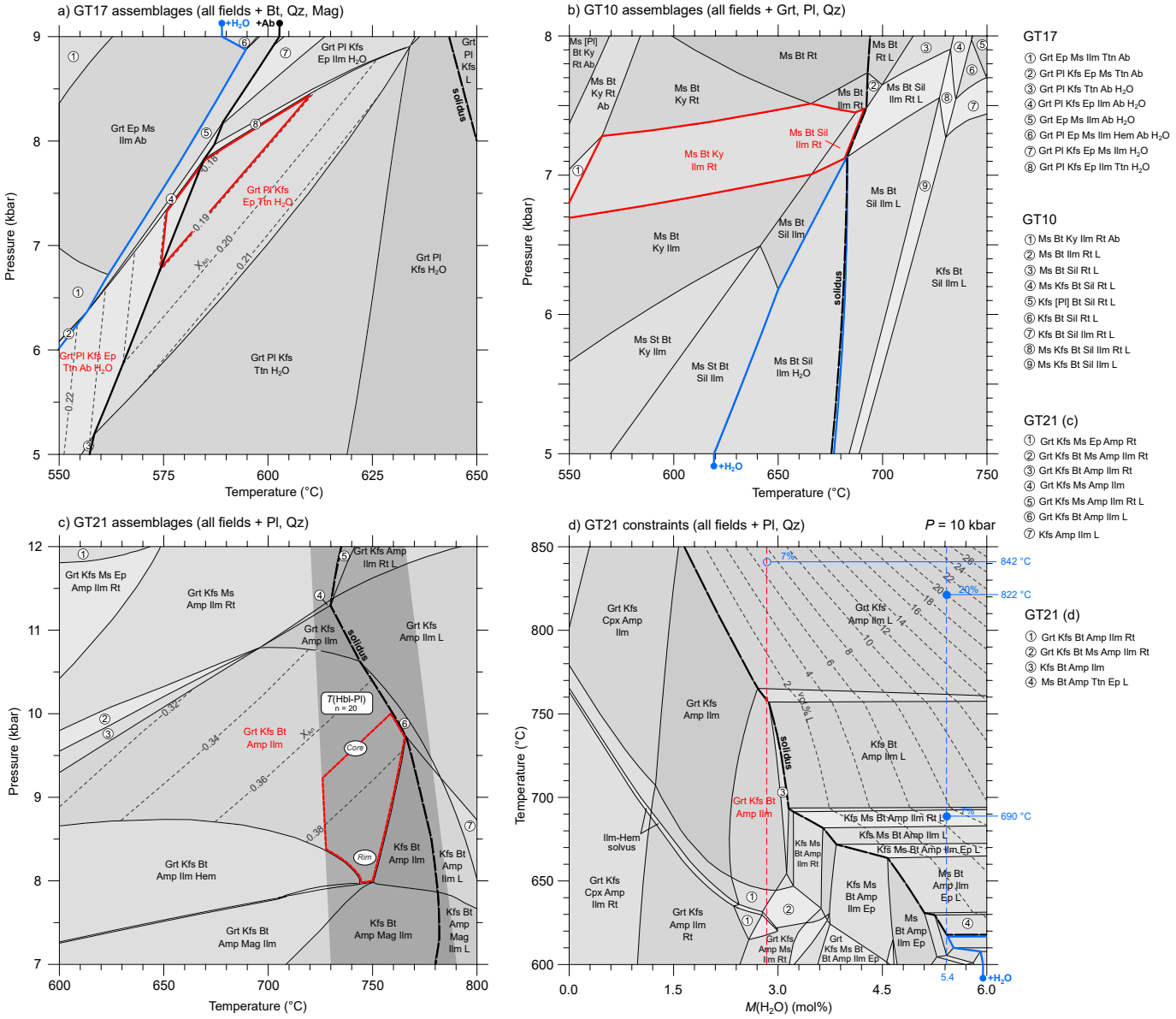


Figure 3: Phase equilibrium modelling results for samples from the Sole Thrust and Grenville Frontal Thrust Zone. (a-c) *P*–*T* pseudosections for Grt-Ep psammite sample GT17 (a), Grt-Ky-Sil schist GT10 (b) and Grt amphibolite GT21 (c). The identified thermal peak assemblages are shown as red text. Prograde to peak-pressure assemblage fields (kyanite-stable) are shown for GT10. Square brackets enclose minerals that are absent from the quoted assemblage. Isopleth contours are shown for X_{An} in oligoclase for samples GT17 (a) and GT21 (c). The vertical grey band in (c) encompasses the hornblende-plagioclase temperature estimates from sample GT21 (n = 20). (d) T–$M(\mathrm{H_2O})$ pseudosection contoured for vol.% melt. Annotations are: the zero-mode isoline for $\mathrm{H_2O}$ (blue line), the $M(\mathrm{H_2O})$ for minimum saturation (dashed blue line), melt proportion at 750 °C (open circle) and temperatures for 7% and 20% melt (closed circles), and the $M(\mathrm{H_2O})$ in (c) (red dashed line).

4.3 Garnet-kyanite-sillimanite schist GT10 (Sole Thrust zone)

Sample GT10 was obtained ~1 km southeast of the Sole Thrust (Fig. 1d), from a mica-rich layer within a southeast-dipping unit of interbedded psammite and pelitic schist. The analysed schist is medium-grained (~1 mm) and comprises: muscovite (37 vol.%), quartz (27 vol.%), garnet (11 vol.%), biotite (11 vol.%), plagioclase (7 vol.%), chlorite (3 vol.%), K-feldspar (1 vol.%) and accessory kyanite, apatite, rutile, ilmenite, monazite, zircon and Fe-sulfides.

Garnet forms up to centimetre-sized anhedral grains that are wrapped by a matrix fabric defined by aligned mica flakes (Fig. 4a). Garnet grain interiors are compositionally zoned and comprise relict core domains ($Alm_{67}Prp_{14}Sps_{12}Grs_{7}$) that transition smoothly outward to inner-rim compositional plateaus ($Alm_{73}Prp_{15}Sps_{6}Grs_{6}$). Garnet has more Fe-rich and Mg-poor outer rims. Inclusions consist of quartz, biotite, muscovite, kyanite, rutile and ilmenite. Kyanite inclusions only occur in the rim region of garnet. Muscovite (Si = 3.03-3.12 cpfu) displays two contrasting forms: ragged, fine-grained aggregates ('Ms_1') and coarser subhedral plates ('Ms_2')(Fig. 4b). Matrix biotite (X_{Mg} = 0.44-0.49) is typically finer-grained compared to Ms_2 and is replaced by chlorite (X_{Mg} = 0.43-0.48). Kyanite forms distributed anhedral grains surrounded by muscovite, whereas sillimanite is intergrown with biotite and quartz. These mineral relationships are consistent with the reaction mechanisms proposed by Carmichael, 1969 that collectively achieve the kyanite–sillimanite transition, but use mica phases as nucleation templates for kinetic reasons. The quartz-biotite-sillimanite aggregates are deformed into folds and overgrow ragged, fine-grained muscovite ('Ms_1') in garnet pressure shadows—all these phases are overgrown by coarser Ms_2 plates (Fig. 4b). Plagioclase is oligoclase in composition (X_{An} = 0.27-0.32) and forms folded centimetre-scale segregations with quartz in garnet strain shadows. Minor K-feldspar forms ragged, altered grains and is intergrown with plagioclase. Rutile occurs mainly in garnet due to varied replacement by ilmenite in the matrix, but faceted matrix rutile is also observed (Fig. 4a). Ilmenite occurs in both garnet and the matrix.

Garnet, muscovite (Ms_1), quartz, biotite, plagioclase, sillimanite, rutile and ilmenite are interpreted as the thermal-peak assemblage, with kyanite additionally having been present during prograde metamorphism. Chlorite overgrows biotite and muscovite Ms_2 cross-cuts folded fabrics—both phases are therefore interpreted to relate to retrogression. K-feldspar is interpreted as detrital based on its ragged, altered appearance.

A P–T pseudosection constructed for sample GT10 (Fig. 3b) contains the kyanite field (red text) and the sillimanite field towards higher temperature. The two fields span a broad temperature range (540–690 °C) and a relatively narrow pressure range (6.7–7.5 kbar). The kyanite field is bound at lower T by albite coming in, at lower P by rutile leaving and at higher P by ilmenite leaving. The sillimanite field is bound at higher T by the solidus, at lower P by rutile leaving and at higher P by sillimanite leaving. The location of these fields indicates that sillimanite joined the assemblage at peak-temperature conditions of 7.3±1 kbar and 678±50 °C. The assemblage is interpreted to have been near fluid saturation based on the occurrence of an adjacent H_2O-bearing field (blue line, Fig. 3b).

4.4 Garnet amphibolite GT21 (Britt Domain)

Sample GT21 was obtained ~18 km southeast of the Sole Thrust (Fig. 1d). The sample is medium-grained (~1 mm) and comprises: plagioclase (53 vol.%), amphibole (15 vol.%), biotite (14 vol.%), quartz (10 vol.%), garnet (4 vol.%) plus K-feldspar, scapolite, apatite, hematite (1 vol% each). Accessory phases include chlorite, allanite, titanite, calcite, zircon,

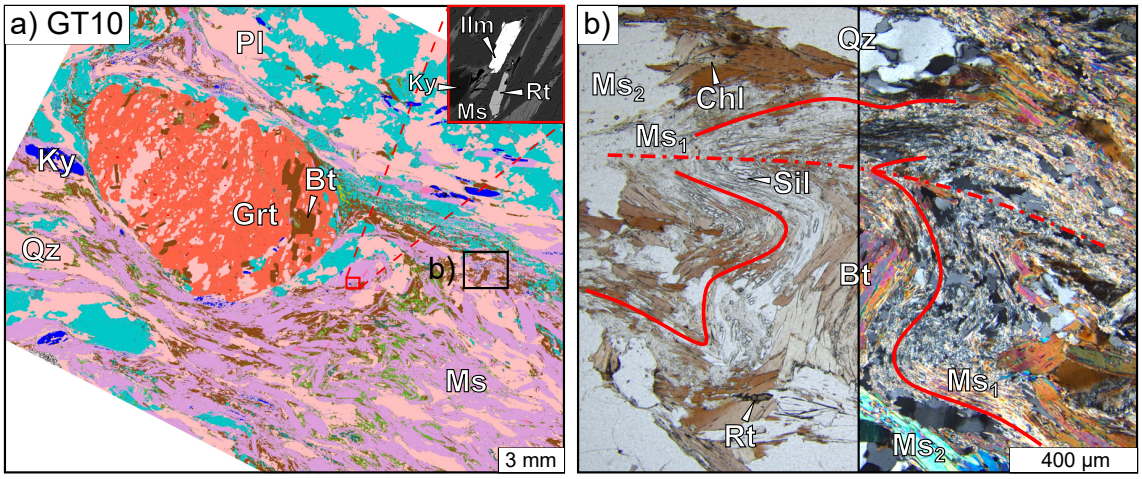


Figure 4: Sample GT10 petrography. (a) QEMSCAN phase map. (b) Split plane- and cross-polarised photomicrograph of the area in (b), focusing on an early fold of sillimanite, biotite and quartz.

ilmenite and Fe-sulfides.

Plagioclase is andesine in composition (X_{An} = 0.37-0.40). Inclusions are common and consist of quartz, amphibole, apatite, biotite and allanite. Amphibole is pargasite in composition and forms anhedral grains embayed by quartz and plagioclase (Fig. 5a,b). Inclusions are common and consist of quartz, plagioclase, apatite, scapolite, biotite, allanite and zircon. Biotite (X_{Mg} = 0.46-0.50) forms subhedral laths. Garnet forms anhedral grains up to 3 mm in diameter embayed by plagioclase. Garnet exhibits uniform composition ($\mathrm{Alm_{51}Grs_{29}Prp_{15}Sps_{5}}$) except at grain margins ($\mathrm{Alm_{52}Grs_{24}Prp_{14}Sps_{10}}$). Garnet contains abundant heterogeneously-distributed inclusions consisting mainly of quartz, biotite, apatite and plagioclase. Hematite forms anhedral grains with ilmenite as lamellae and coronas. Scapolite is anhedral, shares straight grain boundaries with matrix phases and is partially replaced by patchy muscovite. K-feldspar is faceted but is partially replaced by biotite. Chlorite and titanite locally overgrow biotite.

The interpreted peak metamorphic assemblage is plagioclase, amphibole, biotite, quartz, garnet, scapolite, K-feldspar and hematite-ilmenite (i.e. a solid solution precursor to the observed lamellae microstructures). Chlorite and titanite are interpreted as retrograde phases due to their anhedral habit and common association with patchy replacement microstructures.

A P–T pseudosection for sample GT21 (Fig. 3c) shows that the interpreted peak assemblage relevant to the model system (i.e. excluding S-bearing phases, leaving plagioclase, amphibole, biotite, quartz, garnet, K-feldspar and hematite-ilmenite) is situated within a broad area of P–T space situated between 8.0–10.5 kbar and <600 to 770 °C (red text). The stability field is bound at lower P by the hematite-ilmenite solvus. Crossing of the solvus during retrograde conditions is consistent with observed lamellar intergrowths of these phases in thin section. The P–T pseudosection therefore successfully matches both the interpreted assemblage and oxide microstructures. The peak field is also bound at lower T/higher P by biotite leaving and rutile joining the assemblage, and at higher T by the fluid-undersaturated solidus and by garnet leaving the assemblage. Contours for X_{An} exhibit a match with oligoclase core compositions at up to 10 kbar and for rim compositions down to 8 kbar. The plagioclase zoning implies sample re-equilibration during

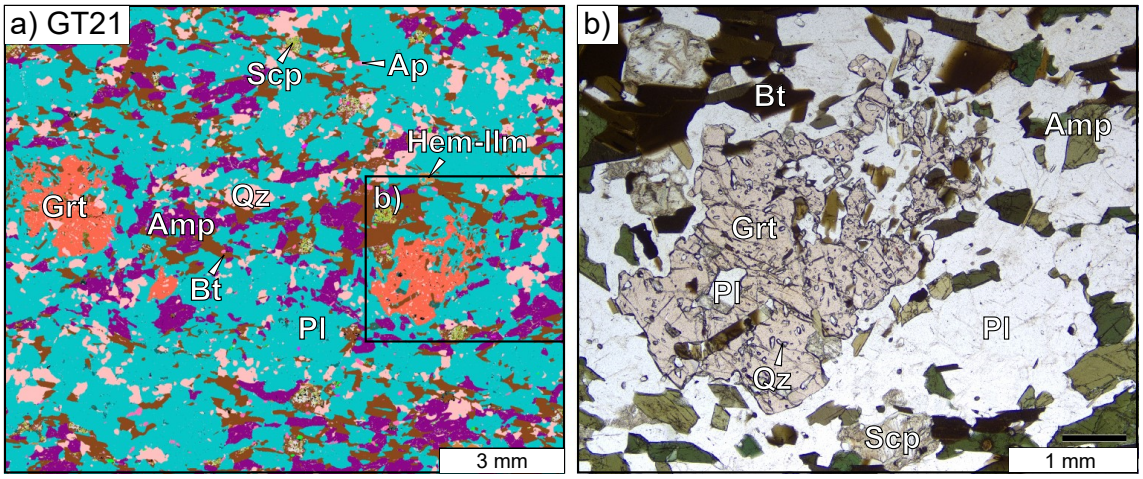


Figure 5: Sample GT21 petrography. (a) QEMSCAN phase map. (b) Plane-polarised photomicrograph of the boxed area in (a).

decompression from peak pressure conditions. Hornblende-plagioclase temperatures (n = 20) were calculated using rim composition pairs. Both minerals exhibit uniform compositions within individual grains, implying preservation of the main equilibrium temperature conditions. Superposition of the hornblende-plagioclase equilibration temperature and the region of oligoclase compositions further constrains the range of conditions to 8.0–10 kbar and 720–765 °C (red outline).

4.5 Garnet-clinopyroxene amphibolite GT36 (Britt Domain)

Sample GT36 was sampled ~33 km southeast of the Sole Thrust (Fig. 1d) from a medium-grained (~0.5-1 mm) mafic body. Two main mineralogical domains are observed: one of garnet, clinopyroxene and plagioclase ('Grt-Cpx domain'), and a second of dominantly amphibole and plagioclase ('Amp domain') (Fig. 6. The Grt-Cpx domain typically forms elongated patches within the more continuous Amp domain. Centimetre-scale plagioclase grains with garnet coronae are also observed and are oriented broadly parallel with the Grt-Cpx patches (Fig. 1a). Based on the mineralogy and outcrop-scale observations, the plagioclase grains are interpreted as phenocrysts from a mafic igneous protolith.

The analysed thin section, which includes both mineralogical domains in the sample (minus the centimetre-scale plagioclase phenocrysts), comprises plagioclase (39 vol.%), amphibole (34 vol.%), garnet (9 vol.%), clinopyroxene (6 vol.%), biotite (3 vol.%), quartz (2 vol.%), ilmenite (2 vol.%), apatite (1 vol.%), K-feldspar (1 vol.%), plus accessory muscovite, titanite, zircon, epidote, chlorite and Fe-sulfides. The compositions of the mineral phases are discussed for the sample as a whole given that they remain chemically consistent in all domains, with only the assemblage and the modes varying.

Amphibole occurs principally in the Amp domain (Fig. 6b,c) where it forms a granular mosaic with equigranular matrix plagioclase, and is pargasite in composition. Matrix plagioclase is antiperthitic and has an oligoclase composition (X_{An} = 0.22-0.37). Plagioclase also forms oligoclase coronas surrounding garnet. The plagioclase phenocrysts were not analysed. K-feldspar occurs as lamellae within antiperthite throughout the sample and as faceted matrix grains within the Grt-Cpx and Amp domains. Garnet forms anhedral grains up to 500 μm in diameter with uniform composition ($Alm_{59}Grs_{21}Prp_{17}Sps_3$). Garnet is

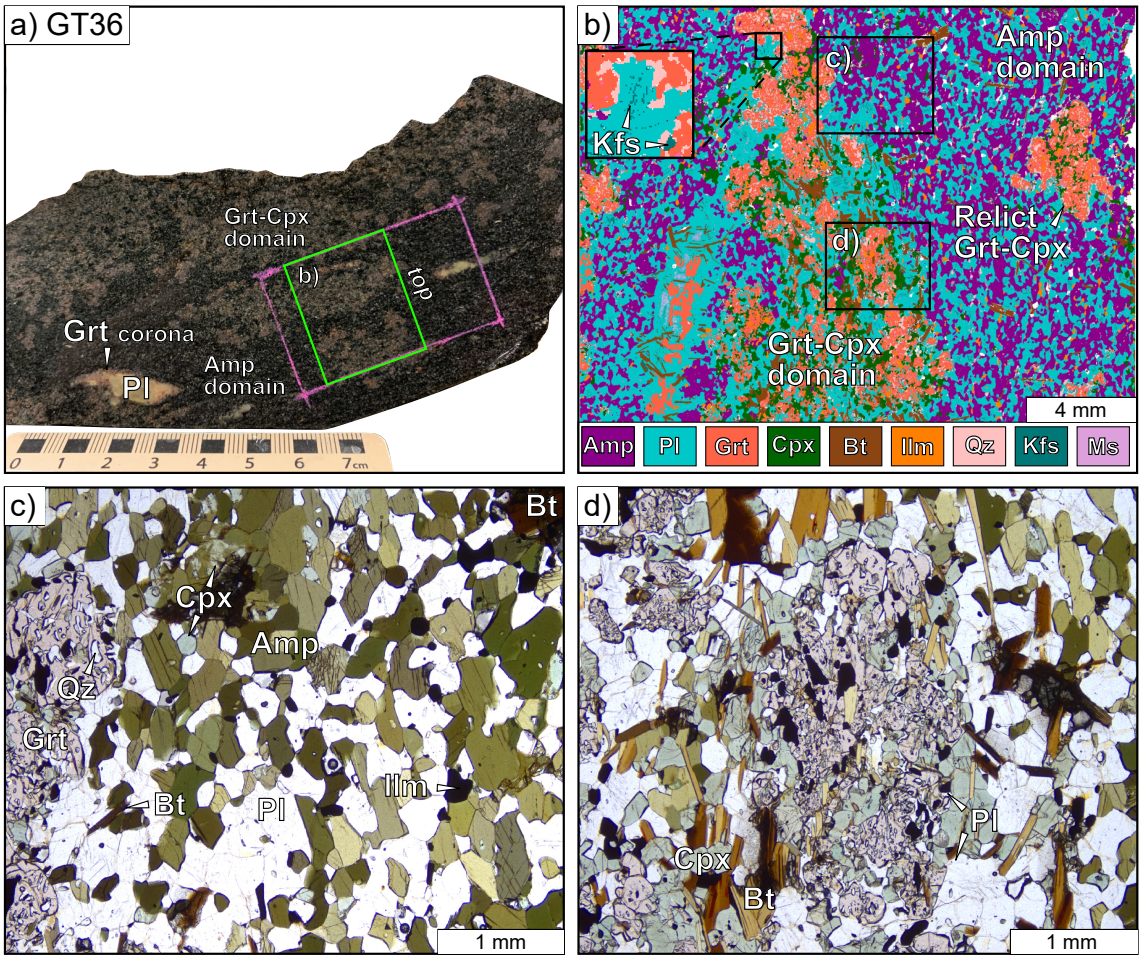
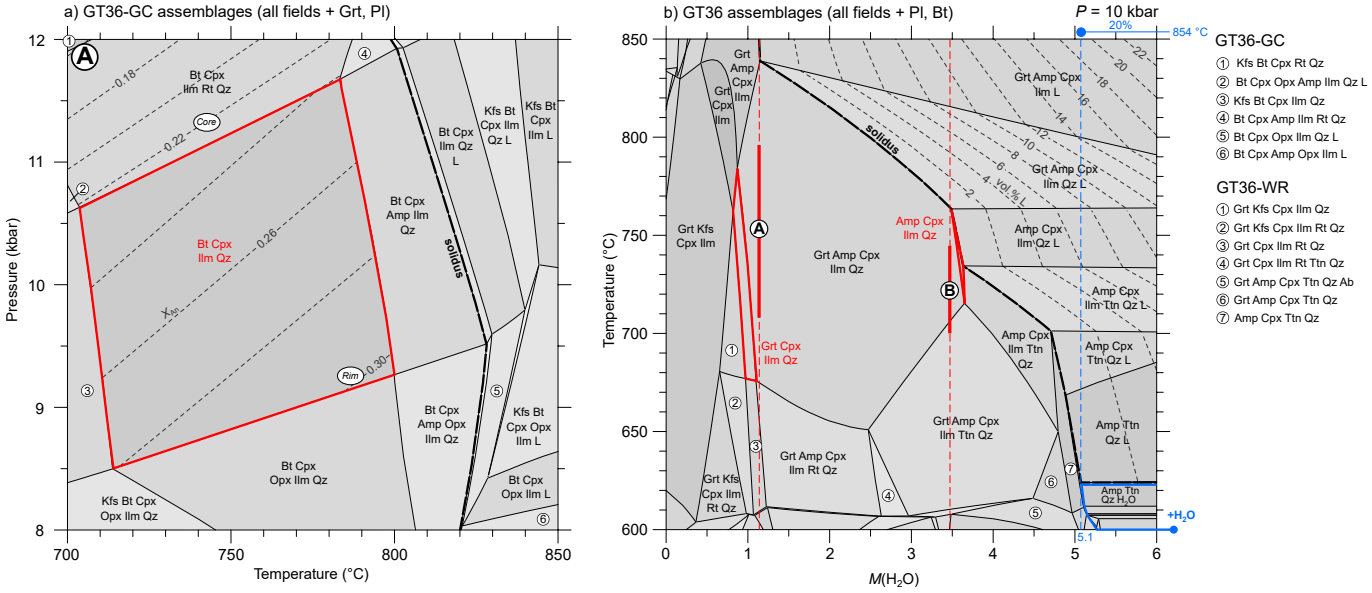


Figure 6: Sample GT36 petrography. (a) Cut slab showing the three fabric components of the sample: plagioclase phenocrysts, garnet-clinopyroxene-rich domains and amphibole-rich domains. (b) QEMSCAN phase map of the green boxed area in (a). The full thin section area is enclosed by the pink box marked on the slab. (c) Plane-polarised photomicrograph of the boxed area in (b), centred on the Amp domain. Note the faceted margins of matrix amphibole and plagioclase. (d) Photomicrograph as in (c) but focused on an anhedral garnet poikiloblast in the Grt-Cpx domain.



heterogeneously distributed, locally in the Amp domain (Fig. 6b) and as aggregates with clinopyroxene in the Grt-Cpx domain (d), and as coronae around plagioclase phenocrysts (a). Garnet is inclusion rich and hosts quartz, clinopyroxene, ilmenite, hematite, biotite, apatite and sulfides—the same as the matrix phases of the Grt-Cpx domain. Volumetrically minor, inclusion-poor garnet occurs as coronae surrounding plagioclase phenocrysts and are chemically indistinguishable from the larger anhedral grains. Clinopyroxene is heterogeneously distributed and shares straight grain boundaries with the matrix phases throughout, except in places within the Amp domain where it is replaced by amphibole. Clinopyroxene is diopside in composition and exhibits elevated jadeite content in the grain cores ($Wo_{40}En_{30}Fs_{17}Jd_7Ae_5$). Biotite ($X_{Mg}$ = 0.50-0.52) occurs in both domains, forming aligned subhedral laths in the Grt-Cpx domain (Fig. 6d) and unoriented laths in the Amp domain (b,c). Ilmenite shares straight grain boundaries with the matrix phases. Titanite forms thin coronae replacing ilmenite rims, and is interpreted as retrograde. Muscovite, epidote and chlorite are patchy and are associated with fractures.

The interpreted equilibrium assemblage for the Grt-Cpx domain is plagioclase, K-feldspar, clinopyroxene, garnet, biotite, ilmenite and quartz based on their shared grain boundaries. The equilibrium assemblage for the Amp domain is amphibole, plagioclase, K-feldspar, clinopyroxene, quartz, ilmenite and biotite based on the granoblastic texture. Garnet in the Amp domain is interpreted as a relict phase based on its anhedral habit and clustered occurrence with clinopyroxene–both phases being more abundant in the Grt-Cpx domain. Muscovite, epidote and chlorite are interpreted as retrograde phases. The large plagioclase grains are interpreted as phenocrysts since they predate garnet growth, including as coronae (Fig. 6a). The Amp domain is interpreted to have formed via fluid-enabled re-equilibration of the Grt-Cpx domain based on the consistent mineral assemblage and mineral compositions in the two domains, and the amphibole-after-clinopyroxene replacement textures in the Amp domain (e.g. Fig. 6c). The textural separation of these domains in Fig. 6a likely results from migration of a fluid front through the grain boundary network of an originally Grt-Cpx dominated matrix (e.g. Whyte et al., 2021).

A P–T pseudosection for the Grt-Cpx domain (Fig. 7a) shows that the closest match to the interpreted peak assemblage is situated within an area of P–T space encompassing 8.5–11.5 kbar and 700–800 °C (red text). The P–T field in Fig. 7a is bound at lower

Figure 7: Phase equilibrium modelling results for sample GT36 from the Britt Domain. (a) P–T pseudosection for the Grt-Cpx domain (GT36-GC) with the interpreted peak-metamorphic assemblage indicated by red text and outline. Isopleth contours are shown for X_{An} in oligoclase (with X_{An} = 0.22 to 0.37 from core to rim) and constrain growth of grain cores at the upper-pressure limit of the assemblage field and rims towards lower pressures. (b) T–$M(\mathrm{H_2O})$ pseudosection produced using a compositional average of GT36-GC and GT36-A (i.e. GT36; Table 3). The assemblage fields for the two domains are indicated by red text and outlined regions. The red bars show the temperature ranges from pseudosection (a) and hornblende-plagioclase thermometry applied to the Amp domain, both at 10 kbar. Annotations are as described earlier for T–$M(\mathrm{H_2O})$ plots.

P by orthopyroxene joining the assemblage, at higher P by rutile joining, at lower T by K-feldspar joining and at higher T by amphibole joining. For analysed plagioclase core-to-rim compositions in the range X_{An} = 0.22 to 0.37, plotted isopleth contours for X_{An} suggest pressures of between ∼11.5 to 9 kbar, which overlaps with the rutile-stable field at higher pressure. The isopleth constraints are interpreted to indicate attainment of peak-pressure conditions at the upper end of the matching assemblage field, at 10.5–11.5 kbar.

4.6 Garnet metatexite GT45 (Britt Domain)

Sample GT45 was obtained ∼64 km southeast of the Sole Thrust (Fig. 1d) from an outcrop of predominantly mafic gneiss. Based on petrological criteria discussed below (Sawyer, 2008), the outcrop is classified as a metatexite, composed of melanosome with more minor leucosome material (following the nomenclature of Mehnert (1968)). The study sample is medium-grained (∼0.1-1 mm) and granular (Fig. 8a). The modal contents are: plagioclase (48 vol.%), amphibole, (30 vol.%), quartz (9 vol.%), K-feldspar (7 vol.%), biotite (4 vol.%), magnetite (1 vol.%) and accessory garnet, apatite, ilmenite, pyrite, zircon, calcite and titanite.

Plagioclase is oligoclase in composition (X_{An} = 0.26-0.32) and antiperthitic. It forms grains ∼0.1-0.7 mm across with lobate grain boundaries—the largest grains mantle anhedral matrix phases (Fig. 8b). K-feldspar forms highly irregular grains, commonly featuring low dihedral angles and co-occurring with myrmekite (Fig. 8c). Amphibole is pargasite in composition and forms anhedral grains. Biotite (X_{Mg} = 0.44-0.50) occurs as subhedral laths. Garnet forms relict grains up to 3 mm in diameter, surrounded by plagioclase (Fig. 8a,b,d). Garnet has inclusions of quartz, magnetite and biotite. Garnet grains exhibit uniform composition ($\mathrm{Alm_{51}Grs_{30}Prp_{11}Sps_8}$) other than at grain margins ($\mathrm{Alm_{50}Grs_{28}Prp_9Sps_{13}}$). Magnetite, ilmenite and pyrite are anhedral or share straight grain boundaries with matrix phases. Titanite replaces biotite and ilmenite.

The interpreted equilibrium assemblage is plagioclase, amphibole, quartz, K-feldspar, biotite, magnetite and ilmenite based on their shared grain boundaries. Plagioclase and K-feldspar display microstructures consistent with crystallised in-situ melt, notably cuspate-lobate grains forming optically continuous frameworks, which enclose garnet and amphibole (Fig. 8b), and myrmekite textures (red circle, Fig. 8c) (Feng et al., 2021; Sawyer, 2001; Holness and Sawyer, 2008). A minor melt phase is thus interpreted as part of the equilibrium assemblage. Relict garnet and melt are interpreted to have co-existed at metamorphic peak conditions, prior to the garnet-absent retrograde overprint. Given the

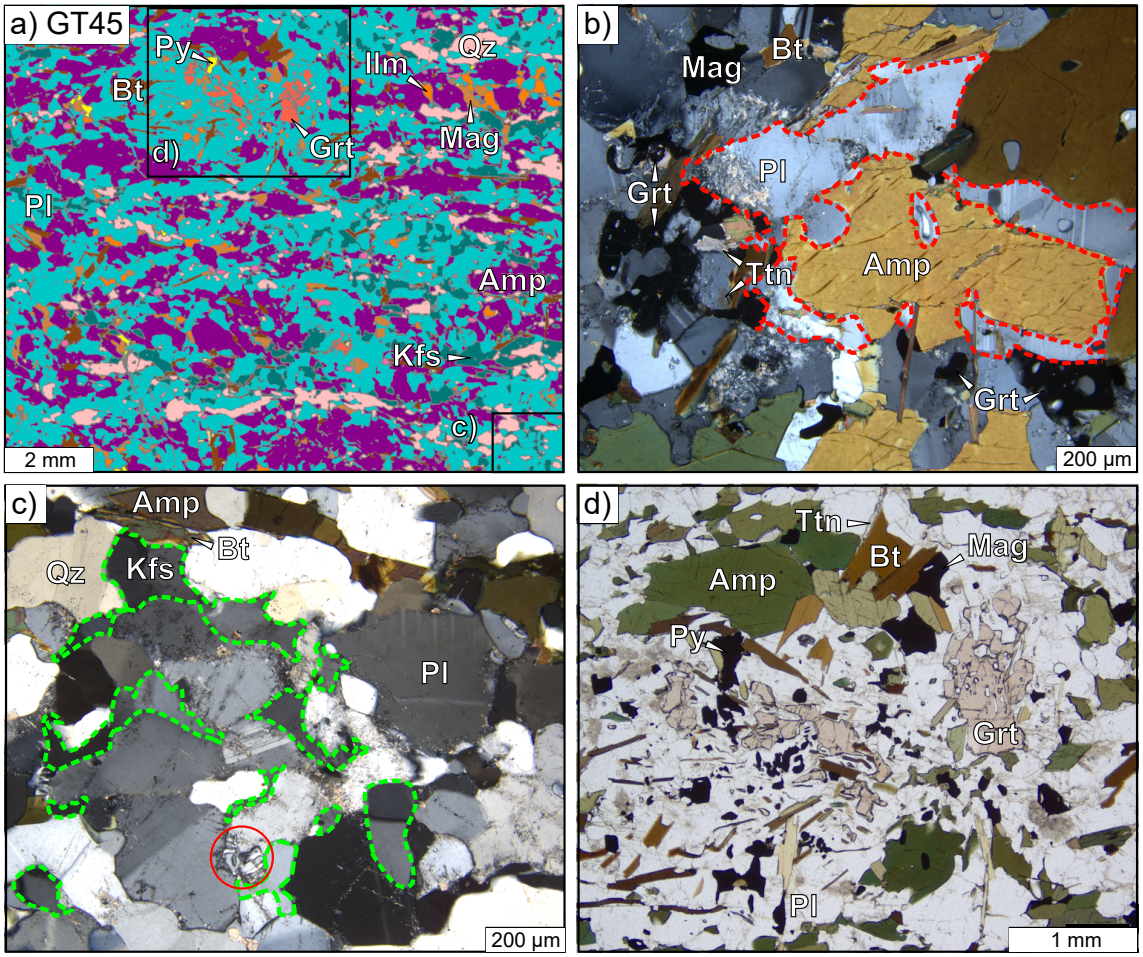


Figure 8: Sample GT45 petrography. (a) QEMSCAN phase map. (b) Cross-polarised photomicrograph highlighting a large plagioclase grain (red dash), interpreted as part of the melt phase, surrounding an amphibole lath. (c) Cross-polarised photomicrograph of the boxed area in (a), showing the cuspate morphology of K-feldspar (green dash). The red circle encloses a myrmekitic intergrowth of plagioclase and quartz. (d) Plane-polarised photomicrograph of the boxed area in (a), centered on two relict garnet porphyroblasts.

absence of peritectic phases associated with biotite and/or amphibole dehydration melting (e.g. orthopyroxene) and the abundance of biotite and amphibole, the inferred melt phase was likely the product of water-fluxed melting (Dyck et al., 2020).

A P–T pseudosection for the melanosome portion of sample GT45 (Fig. 9) shows that the interpreted equilibrium assemblage is located at 7.0–7.5 kbar and 730–810 °C (red text and outline). The field is bound at lower P by K-feldspar leaving the assemblage, at higher P by magnetite leaving, at lower T by the fluid-undersaturated solidus and at higher T by biotite leaving and orthopyroxene joining. The temperature range is corroborated by superimposed hornblende-plagioclase temperature estimates (n = 18).

The garnet plus melt bearing assemblage interpreted from petrographic observations is unbound at the upper P–T limit of the plot extent (green outline). A best estimate for peak conditions in this large field is placed by the intersection of the hornblende-plagioclase temperatures and the X_{An} contour matching the analysed oligoclase core composition, at ~11 kbar and 750 °C.

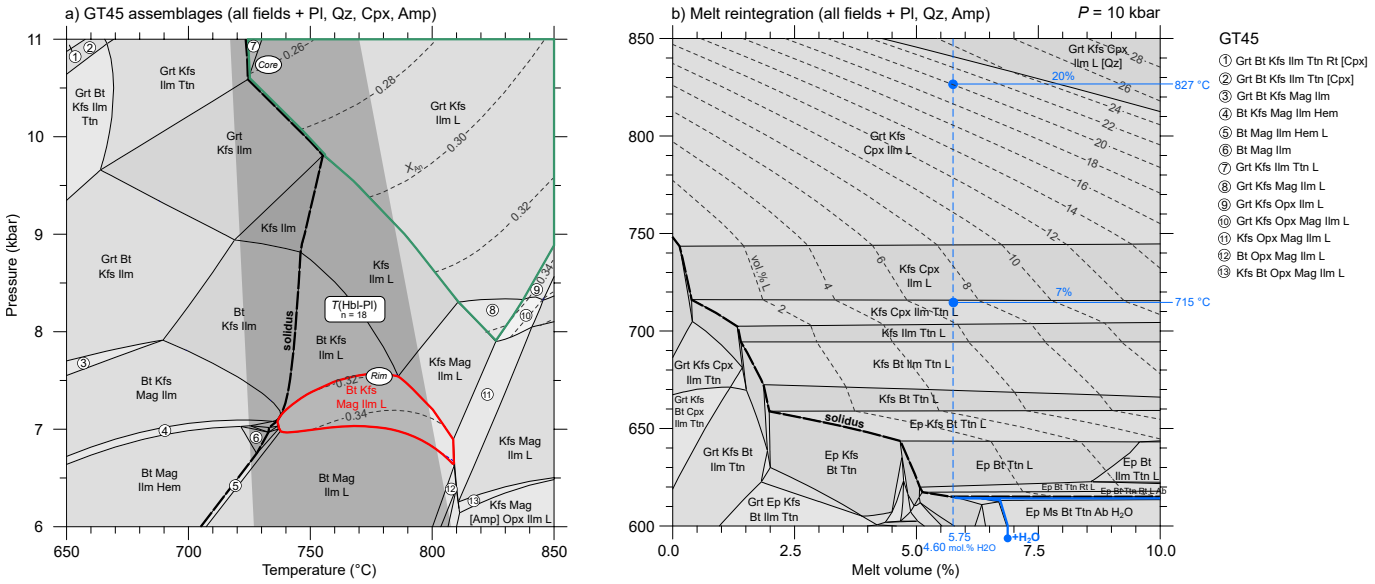


Figure 9: Phase equilibrium modelling results for sample GT45 from the Britt Domain. (a) P–T pseudosection with the interpreted equilibrium assemblage indicated by red text and outline. Isopleth contours are shown for X_{An} in oligoclase, with $X_{\mathrm{An}} = 0.26$ corresponding to grain cores in the garnet plus melt stable field (green outline), and $X_{\mathrm{An}} = 0.32$ to the main garnet-absent equilibrium assemblage (red outline). Hornblende-plagioclase temperatures are superimposed and further refine metamorphic peak conditions to just above the solidus. (b) T–X_{melt} pseudosection contoured for vol.% melt. Annotations are as described earlier for T–$M(\mathrm{H_2O})$ plots.

A T–X_{melt} plot shows that saturation of the solidus occurs for a reintegrated melt volume of 5.75%, which is the best estimate for maximum melt generation. Since petrographic observations suggest continued melt presence down to retrograde conditions of ~7 kbar, the maximum volume of melt at saturation could very well have been higher, promoting melt loss.

4.7 Garnet-kyanite metatexite GT60 (Britt Domain)

Sample GT60 was sampled ~85 kilometres southeast of the Sole Thrust (Fig. 1d). The outcrop and associated sample (Fig. 10a,b) display migmatitic textures with alternating coarse-grained leucocratic layers and smaller volume melanocratic kyanite-rich layers, consistent with melt-related microstructures and phase relations discussed below. The rock is interpreted as a stromatitic metatexite based upon the coherent layered structure (Sawyer, 2008). The locations of the leucosome, melanosome and the unmelted domain (paleosome) as interpreted from the outcrop is shown in Fig. 10a.

Melanosome (GT60-M). The melanosome is fine-grained (0.2 to 0.5 mm) and consists of plagioclase (35 vol.%), K-feldspar (29 vol.%), kyanite (15 vol.%), garnet (8 vol.%), biotite (8 vol.%), muscovite (2 vol.%), quartz (1 vol.%) and accessory chlorite, apatite, rutile, zircon, titanite, monazite, epidote and magnetite (Fig. 10c).

Plagioclase is oligoclase in composition ($X_{\mathrm{An}} = 0.23$-0.25) and forms a granular, polygonal mosaic. K-feldspar ($X_{\mathrm{Or}} = 0.86$-0.91) occurs in two textural settings: as matrix grains with plagioclase, biotite and kyanite, and as coarser grains adjacent to large kyanite blades (Fig. 10d). Some K-feldspar hosts inclusions of faceted to anhedral biotite. Kyanite

occurs as subhedral <1 mm grains within the biotite-rich matrix and as ∼1 cm grains (Fig. 10c,d). Inclusions are common within small (<1 mm) kyanite blades and include mainly K-feldspar and biotite, with minor rutile, monazite, plagioclase and muscovite. Myrmekitic intergrowths of plagioclase and vermicular quartz form rims around kyanite (red circle, Fig. 10c,d). Sillimanite occurs locally as fine-grained aggregates with quartz along feldspar grain boundaries (Fig. 10e). Garnet forms anhedral grains up to ∼3 mm in diameter with a uniform composition ($Alm_{65}Grs_{17}Prp_{15}Sps_3$) except along grain margins ($Alm_{72}Grs_5Prp_{19}Sps_4$). Garnet inclusions are common, heterogeneously distributed, and include muscovite, biotite, K-feldspar, plagioclase, kyanite, monazite and zircon. Biotite (X_{Mg} = 0.45-0.50) forms aligned subhedral laths. Muscovite (Si = 3.11-3.16 cpfu) is patchy and occurs along kyanite margins. Chlorite is also patchy and overgrows biotite. Quartz occurs only as moats surrounding kyanite and sillimanite.

Leucosome (GT60-L). The leucosome is coarse-grained (up to 5 mm) and exhibits a layer-parallel fabric defined by quartz ribbons and the aspect ratio of feldspar grains (Fig. 10c). The modal contents are: quartz (44 vol.%), K-feldspar (42 vol.%), plagioclase (8 vol.%), garnet (4 vol.%), biotite (1 vol.%) and accessory rutile, muscovite, apatite, zircon, baddeleyite, magnetite, and monazite.

Quartz occurs both as ∼1 mm ribbon-shaped grains and <0.3 mm grains (dashed green outline, Fig. 10f). K-feldspar is perthitic (X_{Or} = 0.76-0.92) and forms grains up to ∼1 cm across and <0.3 mm grains. Plagioclase is oligoclase in composition (X_{An} = 0.20-0.24) and forms a fine equigranular matrix with K-feldspar and quartz (<0.3 mm). Quartz, K-feldspar and plagioclase have faceted or lobate grain boundaries (Fig. 10f). Plagioclase and vermicular quartz locally form myrmekitic intergrowths (circled in red, Fig. 10f). Garnet forms anhedral to subhedral poikiloblasts up to ∼5 mm in diameter and exhibits uniform composition ($Alm_{66}Grs_{17}Prp_{14}Sps_3$) except at grain margins ($Alm_{72}Grs_4Prp_{21}Sps_3$). Inclusions in garnet include quartz, feldspars, rutile, biotite, zircon and baddeleyite. Biotite (X_{Mg} = 0.47-0.52) forms subhedral laths at feldspar grain margins and along garnet rims.

Interpreted melanosome assemblage. The interpreted prograde to peak-metamorphic assemblage for the melanosome is plagioclase, K-feldspar, kyanite, garnet, biotite, rutile and melt. Muscovite only occurs as inclusions in garnet and ragged grains in the matrix that are interpreted as prograde and retrograde, respectively. Chlorite replaces biotite and is thus interpreted as retrograde. The quartz moats, sillimanite and myrmekite are interpreted as products of retrograde re-equilibration with melt because of the quartz-poor nature of the rock compared to the leucosome (in which quartz comprises 44 vol.%; see below). The formation of both muscovite and quartz can be explained via the simplified reaction $K\text{-}feldspar + kyanite + H_2O \iff muscovite + quartz$, the reverse of the second aluminosilicate isograd (McLellan, 1985). However, the low proportion of retrograde phases (i.e. quartz and muscovite) is consistent with melt extraction (e.g. to the layer labelled in Fig. 10a) and minimal retrograde modification in the presence of melt.

Sample GT60 was first modelled in terms of its melanosome assemblage, interpreted to have undergone melt loss based on the low degree of retrograde overprinting. A P–T pseudosection in Fig. 11a locates the interpreted assemblage (plagioclase, K-feldspar, kyanite, garnet, biotite, rutile and melt) within a narrow field (red line) centred at 9.5±0.5 kbar and 775±50 °C, in which muscovite-out and corundum-in reactions are shown as superimposed. The former bounds the field at lower T whereas the latter occurs at a higher temperature.

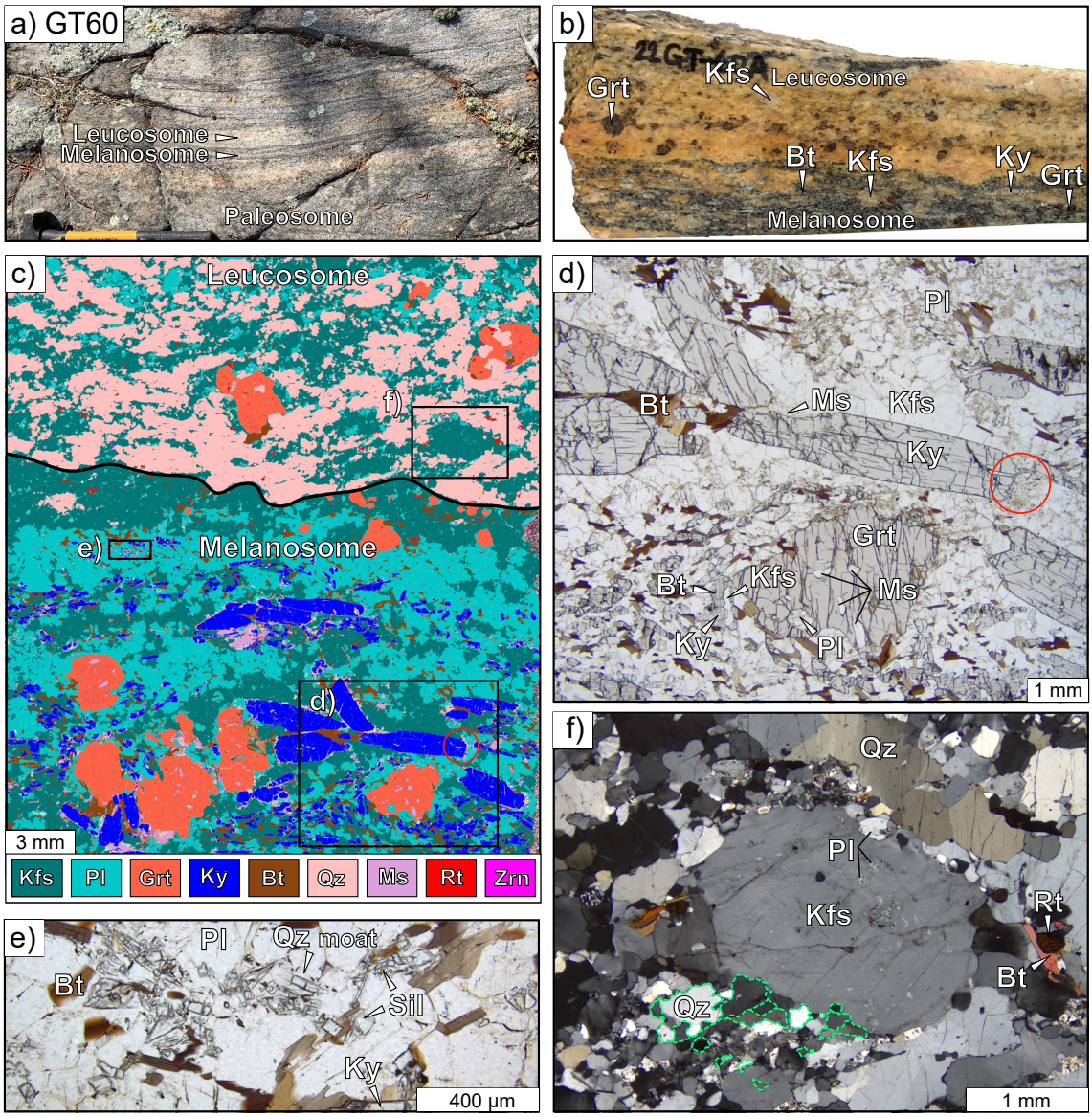


Figure 10: Sample GT60 petrography. (a) Field photo showing the stromatic layering in the metatexite. (b) Cut slab viewed perpendicular to the compositional layering. (c) QEMSCAN phase map of the leucosome-melanosome boundary (black line). (d,e) Plane-polarised photomicrographs of the boxed areas of the melanosome in (c). Panel (e) highlights a quartz-sillimanite aggregate, interpreted as a product of retrograde re-equilibration. (f) Cross-polarised photomicrograph of the area of the leucosome boxed in (c), centred on a melt-crystallised K-feldspar phenocryst. The green dashed lines enclose some of the quartz grains and show the range of grain sizes (e.g. compared to the ∼1 mm grains at the top of the photomicrograph). The red circle encloses a myrmekitic intrgrowth of quartz and plagioclase.

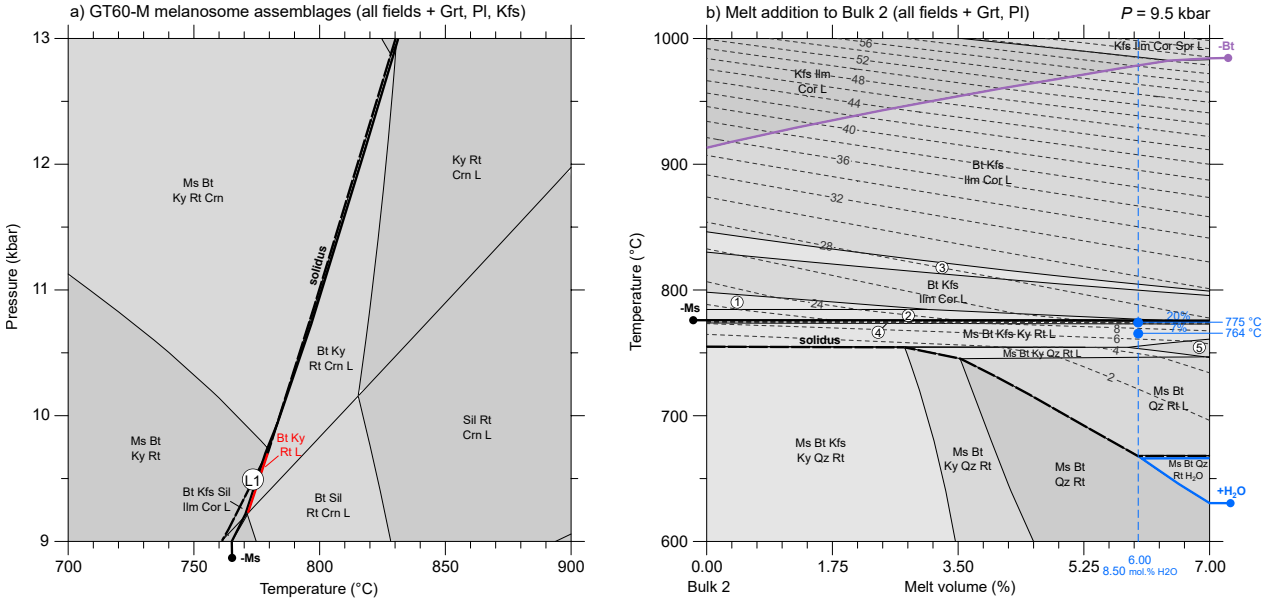


Figure 11: Phase equilibrium modelling results for sample GT60 from the Britt Domain. (a) P–T pseudosection of the melanosome (GT60-M) with the best-matching assemblage field denoted by red text. (b) T–X_{melt} pseudosection ranging from 0 to 7% melt after two batch reintegration steps (see Fig. S3), contoured for vol.% melt. Annotations are as described earlier for T–$M(\mathrm{H_2O})$ plots.

The garnet inclusion assemblage (K-feldspar, muscovite, biotite, plagioclase, kyanite and melt), interpreted as recording prograde conditions, was modelled via a stepwise melt reintegration correction to the melanosome. Based on the 7 vol.% melt connectivity transition of Rosenberg and Handy (2005), batches of this volume proportion were cumulatively integrated into the bulk composition until the fluid-saturated solidus was reached. The first reintegrated composition was calculated using melanosome composition 'GT60-M' (Fig. 11a) plus a melt composition 'L1' located along the fluid-undersaturated solidus, at the average pressure of the identified peak assemblage field (9.5 kbar, red line): Bulk 1 = 0.93[GT60-M] + 0.07[L1]. The second integration uses Bulk 1 plus a melt composition 'L2' determined from the Bulk 1 solidus at 9.5 kbar: Bulk 2 = 0.93[Bulk 1] + 0.07[L2]. The P–T pseudosections for these intermediate integration steps are shown in Fig. S3, with the bulk compositions given in Table 3. A final integration of 6 vol.% is necessary to saturate the solidus at 9.5 kbar, as shown in the T–X_{melt} pseudosection in Fig. 11b. The melt reintegration analysis indicates that ∼3 batches of 7 vol.% melt saturate the solidus, meaning a cumulative melt loss of at least ∼20 vol.% during prograde metamorphism to thermal-peak conditions of 9.5±0.5 kbar and 770±50 °C.

4.8 Epidote-biotite amphibolite GT58 (Shawanaga Domain)

Sample GT58 was sampled 13 km southeast of the Allochthon Boundary Thrust (Fig. 1d). The outcrop features a homogeneous texture and medium grain size (∼0.5-1 mm). The modal contents are: plagioclase (52 vol.%), quartz (21 vol.%), biotite (15 vol.%), K-feldspar (7 vol.%), amphibole (2 vol.%), epidote (1 vol.%) and accessory titanite, muscovite, apatite, chlorite, zircon and magnetite.

Plagioclase is oligoclase (X_{An} = 0.22-0.27) and forms a matrix of subhedral grains with

quartz (Fig. 12a-c). Where in contact with K-feldspar, plagioclase grains have well developed albite mantles (Fig. 12d). K-feldspar is microcline (X_{Or} = 0.93-0.94) and forms irregularly-shaped grains between plagioclase, featuring low-dihedral angles (e.g. the area circled in Fig. 12b,c). Myrmekitic intergrowths of oligoclase and vermicular quartz occur adjacent to some K-feldspar grains (Fig. 12a inset). K-feldspar is interpreted to have crystallised from a former melt phase based upon its textural characteristics (e.g. low dihedral angles; Holness and Sawyer, 2008; Sawyer, 2001). Biotite is subhedral and has X_{Mg} = 0.46-0.48. Amphibole forms anhedral grains embayed by quartz and feldspar, and shares straight grain boundaries with, or is overgrown by, biotite. The composition of the amphibole is pargasite. Epidote (X_{Ps} = 0.26-0.28) forms subhedral to euhedral grains, which commonly appear to cross-cut biotite flakes (Fig. 12c). Titanite is anhedral. Minor muscovite and chlorite are present at the margins, or along cleaveage planes, of biotite.

The interpreted peak metamorphic assemblage is plagioclase, quartz, biotite, K-feldspar (melt), amphibole and titanite based on the interlobate texture at shared grain boundaries. Epidote is interpreted as a retrograde phase because it topotaxially replaces biotite and has a faceted habit that mirrors biotite, compared to the anhedral habit of amphibole (Fig. 12b,c). Albite is also interpreted as retrograde owing to its occurrence as distinct mantles on more calcic plagioclase cores. Muscovite and chlorite are rare (<<1 vol.%) and are present within biotite, and are therefore interpreted as late alteration phases.

A P–T pseudosection in Fig. 13a shows the peak assemblage plus a hematite-ilmenite solid solution, which was not observed in thin section. The combined hematite- and ilmenite-stable fields are bound at lower P by clinopyroxene joining the assemblage, at higher P by rutile joining, at lower T by epidote joining and higher T by titanite leaving. Hornblende-plagioclase temperatures (n = 19) were calculated using rim composition pairs. For the analysed plagioclase compositions of X_{An} = 0.22 to 0.27, isopleth contours for X_{An} suggest likely P–T conditions at the upper-pressure end of the assemblage field, centered at ~9.5±1 kbar and 715±50 °C (red text).

A T–X_{melt} pseudosection in Fig. 13a constrains the minimum melt volume to ≥3.73%, which is consistent with thin K-feldspar grain-boundary films and locally-formed myrmekite intergrowths being the only petrographic observations consistent with melting (Fig. 12a-c).

4.9 Garnet-chlorite schist GT33 (Shawanaga Domain)

Sample GT33 was sampled 16 km southeast of the Allochthon Boundary Thrust (Fig. 1d). The sample is medium-grained (~0.5-1 mm) and exhibits a schistosity defined by aligned biotite (Fig. 14a). The modal proportions are: plagioclase (52 vol.%), biotite (32 vol.%), quartz (7 vol.%), ilmenite (4 vol.%), garnet (2 vol.%), hematite (1 vol.%) and accessory apatite, chlorite, zircon and monazite.

Plagioclase is oligoclase (X_{An} = 0.16-0.18) and forms an equigranular polygonal mosaic. Biotite is euhedral and has X_{Mg} = 0.73-0.74. Garnet forms anhedral to euhedral grains up to ~2 mm in diameter, overgrowing the biotite fabric. Garnet grains are chemically zoned, with a core composition of $Alm_{41}Sps_{33}Prp_{19}Grs_{7}$ and a rim composition of $Alm_{36}Sps_{45}Prp_{10}Grs_{9}$. Inclusions in garnet are common, heterogeneously-distributed, and consist of ilmenite, quartz and plagioclase. Ilmenite is mainly subhedral. Hematite is euhedral and shares straight grain boundaries with ilmenite. Chlorite occurs along biotite

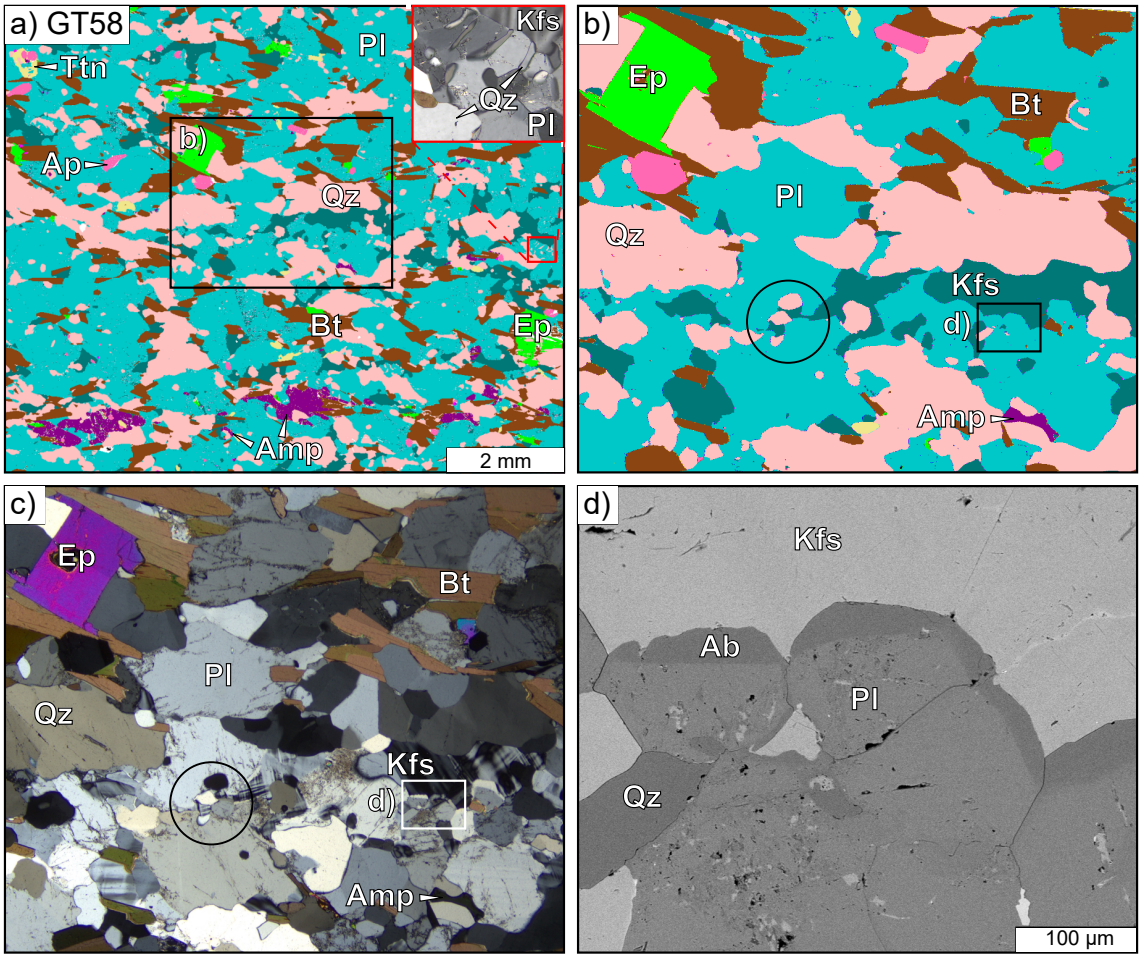


Figure 12: Sample GT58 petrography. (a) QEMSCAN phase map. Inset: cross-polarised light photomicrograph of a myrmekite texture. (b) Phase map of the boxed area in (a), highlighting low-dihedral K-feldspar between neighbouring plagioclase (circled area). (c) Cross-polarised light photomicrograph of panel (b). (d) Back-scattered electron image of the boxed area in (b) and (c), showing late albite mantles on plagioclase, embaying adjacent K-feldspar.

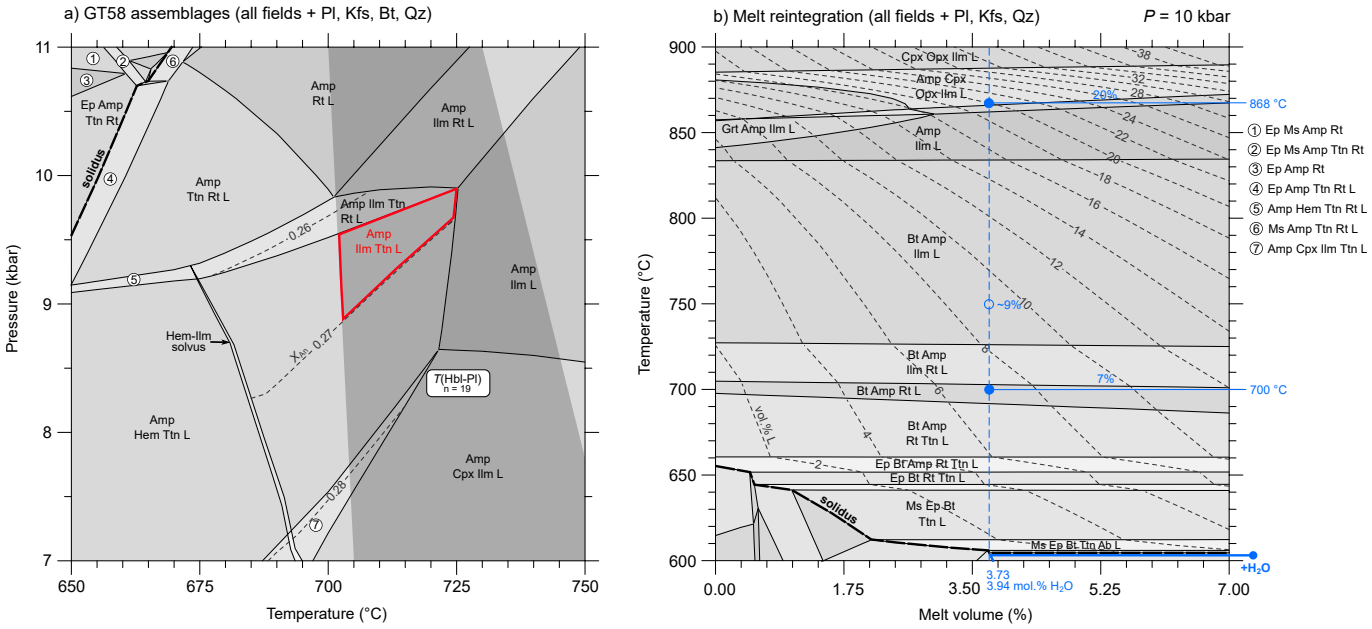


Figure 13: Phase equilibrium modelling results for sample GT58 from the Shawanaga Domain. (a) P–T pseudosection with contours of X_{An} for oligoclase, which has compositions between 0.22 and 0.27. The interpreted peak-metamorphic assemblage plus ilmenite is denoted by the red text, in the region of overlap with hornblende-plagioclase temperature estimates. (b) T–X_{melt} pseudosection contoured for vol.% melt. Annotations are as described earlier for T–$M(\mathrm{H_2O})$ plots.

grain boundaries and within cleavage. Less commonly, chlorite flakes share straight grain boundaries with biotite.

The interpreted peak metamorphic assemblage is plagioclase, biotite, quartz, ilmenite, garnet and hematite based on their shared grain boundaries. Chlorite is interpreted as a retrograde phase, but the faceted habit of some grains suggests it forms part of the equilibrium assemblage. Minor retrogression is evidenced by patchy chlorite replacement of biotite.

A P–T pseudosection for sample GT33 (Fig. 15b) shows that the observed equilibrium assemblage is stable at 4.8–8.5 kbar and 603±50 °C, with additional rutile present at <2 vol.%. The field is bound at lower P by hematite leaving the assemblage, at higher P/lower T by albite joining and higher T by chlorite leaving. A T–$X(\mathrm{Fe^{3+}})$ plot at 6 kbar in Fig. S2e shows that rutile destabilises below $X(\mathrm{Fe^{3+}}) = 0.1$ to 0.2 (originally 0.31) within the temperature window bound at higher T by chlorite-out and lower T by albite-in. For analysed plagioclase compositions of $X_{\mathrm{An}} = 0.16$ to 0.18, plotted isopleth contours for X_{An} suggest a minor refinement in pressure. However, the P–T region defined by the assemblage field boundaries is considered a more robust constraint than the compositional contours owing to the large (∼1 to 2 kbar) spacing and minor increments in associated plagioclase composition.

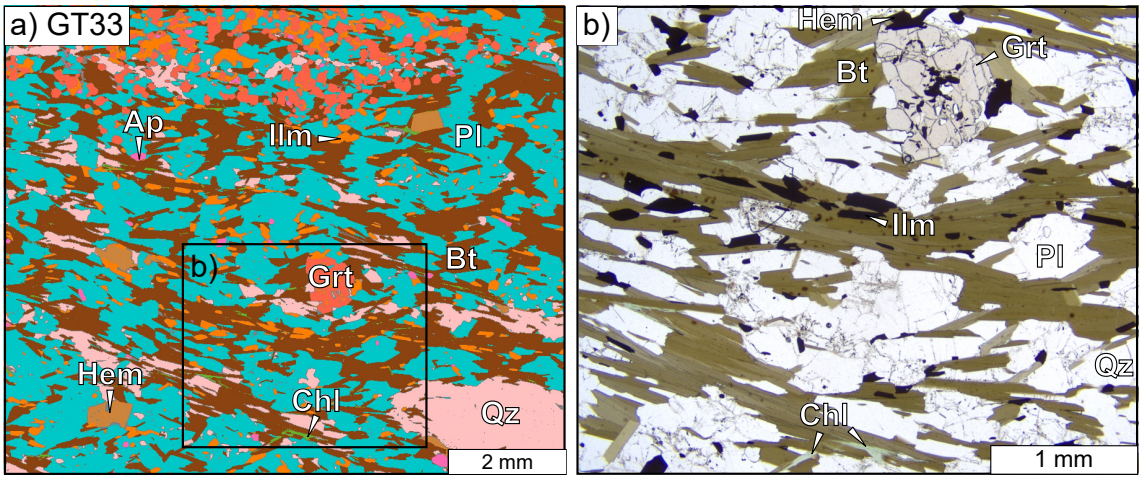


Figure 14: Sample GT33 petrography. (a) AZtecMineral phase map. (b) Plane-polarised light photomicrograph of the boxed area in (a).

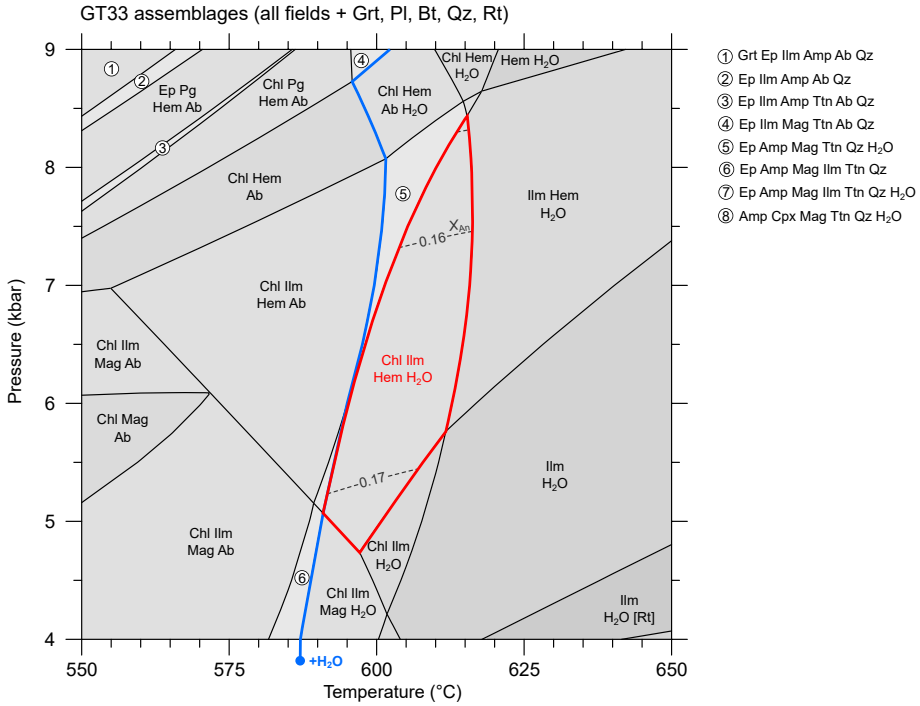


Figure 15: Phase equilibrium modelling result for sample GT33 from the Shawanaga Domain. *P–T* pseudosection of the interpreted retrograde (chlorite-stable) assemblage with contours of X_{An} for oligoclase, which has compositions between 0.16 and 0.18. The equilibrium assemblage is shown by red text, plus rutile which was not observed in thin section.

4.10 P–T results

Our results from pseudosection analyses applied to the eight samples indicate variability in metamorphic conditions between 5–11 kbar and 600–800 °C (black boxes, Fig. 16). Five of the eight samples yield conditions that overlap at 9 to 11 kbar and 700 to 800 °C, with inferred peak pressures of 10 kbar as discussed below. The data further refine the suite of previously-determined thermobarometric estimates from the region, and they form the basis for the T–$X_{\mathrm{melt}}/M(\mathrm{H_2O})$ results synthesised below.

In the GFTZ, the available P–T data vary between 6 to 11 kbar and 600 to 750 °C (Anovitz and Essene, 1990; Davidson, Carmichael, and Pattison, 1990; Bethune and Davidson, 1997; Jamieson, Culshaw, and Corrigan, 1995; Corfu and Easton, 2001) (colour-coded data; Fig. 16a,b). Attainment of ∼10 kbar at 700–750 °C during peak metamorphism is constrained from sample GT21, with the pressures corroborated by GRIPS and GAFS barometry estimates of Anovitz and Essene (1990) from pelitic and mafic rocks, respectively. Isothermal re-equilibration is thought to have occurred at ∼6–7 kbar based on the sample GT10 constraint and metadiabase coronae analysed by Bethune and Davidson (1997) (red data). Both sample GT17 and metadiabase analysed by Jamieson, Culshaw, and Corrigan (1995) (brown) indicate a lower retrograde temperature of 600 °C, in the proximal footwall of the Sole Thrust.

In the Britt domain, pressure data are between 4 to 15 kbar whereas temperatures are 600 to 870 °C across most of the domain and down to 500 °C within 10 km of the ABT (Anovitz and Essene, 1990; Tuccillo et al., 1992; Jamieson, Culshaw, and Corrigan, 1995; Ketchum et al., 1994; Chapman, 2017). The majority of data, except adjacent to the ABT (Ketchum et al., 1994) (yellow data), are based on the TWQ method of Berman (1991) applied by Jamieson, Culshaw, and Corrigan (1995) to metadiabase (brown data). The P–T variability is observed across dykes with a similar Grt-Cpx±Opx assemblage, suggesting disequilibrium among selected mineral pairs and/or varied records of retrogression. The highest reported P–T data from Jamieson, Culshaw, and Corrigan (1995) are 12–14 kbar and 840–870 °C, which are consistent in terms of pressures with the estimates by Chapman (2017) (13–15 kbar and 719–785 °C; TWQ method) similarly applied to metadiabase. However, Jamieson, Culshaw, and Corrigan (1995) applied Grt-Hbl thermometry and Grt-Hbl-Pl-Qz barometry to the same equilibrium assemblage, which expanded the possible P–T range down to ∼10 kbar and 610 °C. Chapman (2017) additionally applied Grt-Cpx-Pl-Qz barometry, which also expanded their pressure range to ∼10 kbar. The elevated P–T conditions as reported by Jamieson, Culshaw, and Corrigan (1995) and Chapman (2017) are therefore more variable than quoted by the authors (and as shown in Fig. 16a,b), with the P–T record viably within uncertainty of the estimates from samples GT21, GT36-GC, GT45 and GT60, depending on the thermobarometric approach used. Data in the proximal footwall of the ABT is primarily from Ketchum et al. (1994) (yellow data), who applied TWQ to metagabbro and Grt-Ky-Kfs±Sil gneiss. The mafic and pelitic rocks yield similar conditions of 6.7–10.6 kbar/510–770 °C and 5.2–11.6 kbar/555–820 °C, respectively, indicating that the spread is not correlated with the protolith chemistry. Ketchum et al. (1994) interpreted these wide P–T data to record varied degrees of retrograde re-equilibration across the ABT. Taken together, previous P–T data from the Britt domain show considerable scatter, which we attribute to varied retrogression and choice of thermobarometer and calibration. Retrograde re-equilibration is exemplified by sample GT45 in which the volumetrically-dominant assemblage formed at 7.0–7.5 kbar and 730–810 °C (Fig. 16a,b), with relict (0.2 vol.%) garnet and plagioclase core compositions indicating prior attainment of up to 11 kbar. Pseudosection results from

the remaining samples in the Britt Domain (GT36, GT60) record conditions of 8–11 kbar and 700–800 °C, consistent with the 8–10 kbar/720–765 °C constraint from GT21 in the GFTZ-Britt Domain boundary zone. Pressure overlap amongst these four samples (GT21, GT36, GT45, GT60) is therefore observed at ∼10 kbar, which is the chosen pressure for the T–$X_{\mathrm{melt}}/M(\mathrm{H_2O})$ pseudosections.

In the Shawanaga domain, data vary between 4 to 11 kbar and 500 to 850 °C (Tuccillo et al., 1992; Ketchum et al., 1994; Wodicka, Ketchum, and Indares, 2000), consistent with the variability observed in the proximal footwall of the ABT. Peak pressures in the Shawanaga domain are interpreted to have reached ∼10–11 kbar and 700–830 °C based on the P–T estimate from sample GT58 and separate determinations on a pelitic schist from Wodicka, Ketchum, and Indares (2000) (TWQ method) and Tuccillo et al. (1992) (GASP/GRIPS barometry). These conditions are consistent with those in the Britt domain and imply continuity in metamorphic grade across the ABT. The abundance of data towards 4 kbar and 500 °C, the P–T constraint from sample GT33 and the occurrence of sillimanite (and more subordinate kyanite) in the Shawanaga domain collectively indicate a low-grade overprint of upper amphibolite facies assemblages (Tuccillo et al., 1992; Ketchum et al., 1994; Wodicka, Ketchum, and Indares, 2000). The poly-metamorphic history accords with observed chlorite-after-biotite textures in sample GT33 and the faceted habit of some chlorite (i.e. forming part of the broader equilibration volume; see Fig. 14b). A sufficiently large volume of fluid would have been required to reset thermobarometers across the Shawanaga Domain as suggested by the literature data in Fig. 16.

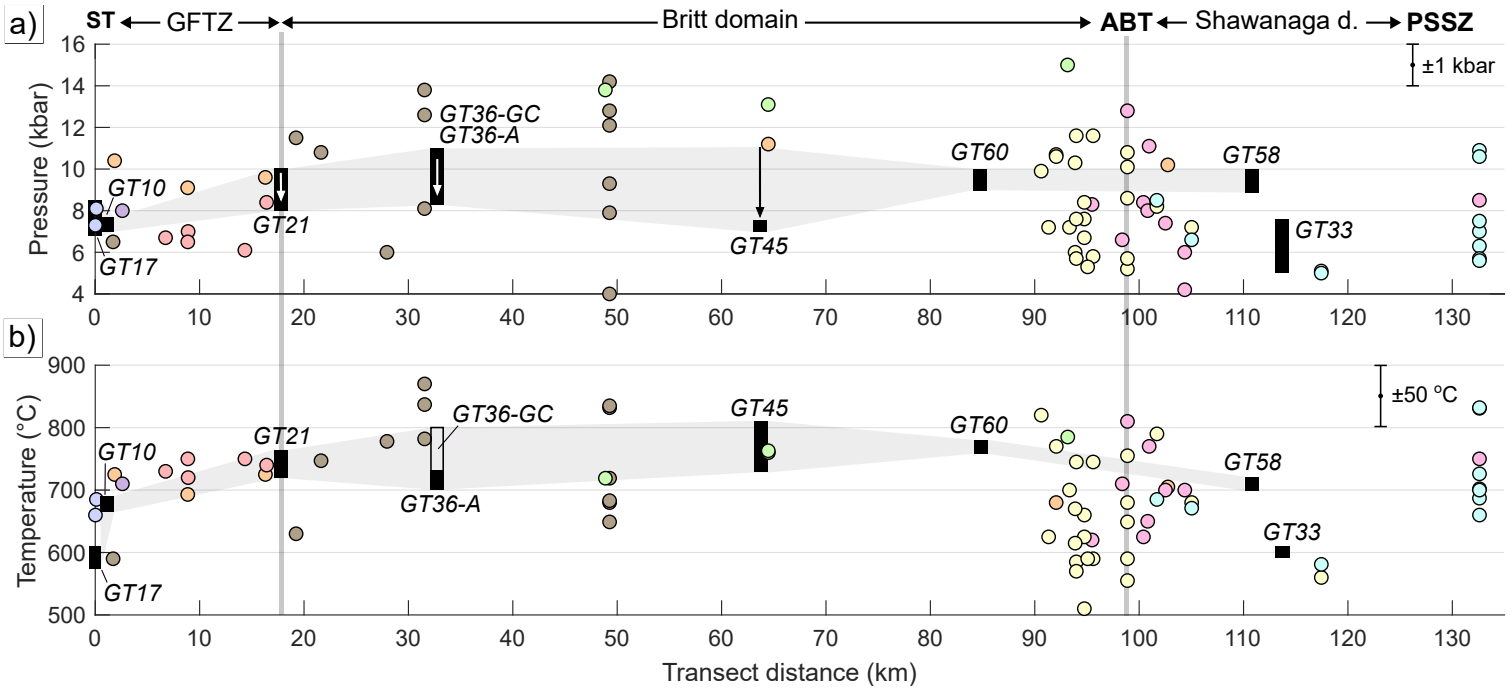


Figure 16: P (a) and T (b) plotted against distance along profile AB (Fig. 1c). The location of all data are shown in Fig. S5; the method of how these date were projected onto profile AB is described in the Supplement. P–T constraints from this work are indicated by black boxes. Uncertainties for all the P and T data are shown by the ±1 kbar and ±50 °C error bars at the right side of the plots. Abbreviations: ST = Sole thrust, ABT = Allochthon Boundary thrust, PSSZ = Parry Sound shear zone.

5 $M(H_2O)$ results

In this section we present constraints on H_2O saturation states of the samples ($f_{sat} = M(H_2O)_{obs}/M(H_2O)_{sat}$) and the effects on the temperatures of the solidi, 7 vol.% melt and 20% melt thresholds. Determinations of $M(H_2O)_{sat}$ and temperatures of threshold melt volumes under conditions of H_2O saturation are from T–X_{melt} and T–$M(H_2O)$ pseudosections at 10 kbar. The fixed pressure is based on the combination of literature and study constraints summarised in the previous section. Constraints of 7%/20% melt temperatures for observed water contents are not shown in the pseudosections but are summarized below in Fig. 17. The 7%/20% melt temperatures were also calculated for the two hydration states at 8 kbar to examine the effects of pressure. 'Saturation' is defined here as the minimum mol.% H_2O required to saturate the solidus, above which free H_2O appears at sub-solidus conditions.

A T–$M(H_2O)$ plot for sample GT21 (Fig. 3d) shows that the temperature constraints from hornblende-plagioclase thermometry at 10 kbar (720 to 765 °C) locate the assemblage at the fluid-undersaturated solidus. Saturation of the solidus occurs at ≥5.4 mol% H_2O, at a lower temperature of ~620 °C. With a stoichiometric water content of 2.82 mol%, the equilibrium assemblage has a saturation factor ($f_{sat} = M(H_2O)_{obs}/M(H_2O)_{sat}$) of 2.82/5.40 = 0.52, which displaces the solidus by +140 °C. Contours of vol.% melt indicate that 7%/20% melt would be produced at 690 °C/822 °C for 5.4 mol% H_2O and 842 °C/894 °C for the stoichiometric content of 2.82 mol%.

For garnet-clinopyroxene amphibolite GT36, a T–$M(H_2O)$ is plotted for the average bulk composition of the two mineralogical domains (Fig. 7c). The plot shows that hydration of the Grt-Cpx domain (from 1.03 to 3.40 mol.%) at c. 710–760 °C is results in the loss of garnet and increase in amphibole/clinopyroxene ratio to produce the Amp domain assemblage. Saturation of the solidus occurs at ≥5.1 mol% H_2O and ~620 °C. These constraints indicate that in the Grt-Cpx domain, f_{sat} = 1.03/5.20 = 0.20 displaces the solidus by +220 °C, and in the Amp domain, f_{sat} = 3.40/5.10 = 0.67 displaces the solidus by +140 °C. Contours of vol.% melt indicate that 7%/20% melt would be produced at 750 °C/854 °C for 5.10 mol% H_2O and 834 °C/931 °C for the stoichiometric content of 3.40 mol% (Amp domain).

Garnet metatexite GT45 was interpreted from a T–X_{melt} in Fig. 9b to have undergone >6 vol.% melting at thermal-peak conditions (between 7 and 10 kbar), close to the 7% melt connectivity threshold (Rosenberg and Handy, 2005). The hydration state of the sample is thus interpreted to record a contribution from melt loss. Saturation of the solidus was determined to occur at ≥4.60 mol% H_2O and ~615 °C. With a stoichiometric water content of 2.55 mol% and saturation level of 4.60 mol% from Fig. 9b, the equilibrium assemblage has f_{sat} = 2.55/4.60 = 0.55, which displaces the solidus by +135 °C. Contours of vol.% melt indicate that 7%/20% melt would be produced at 715 °C/827 °C for 4.60 mol% H_2O. Further melting of the metatexite at 10 kbar would require much higher temperatures of 834 °C/931 °C.

Garnet-kyanite metatexite GT60-M was found to have undergone cumulative melt loss of at least ~20 vol.% based on a melt reintegration analysis in Fig. 11b, to produce the anhydrous phase assemblage observed in thin section with 1.37 mol% H_2O. Saturation of the solidus occurs at ≥8.50 mol% H_2O from the reintegrated melt, yielding f_{sat} = 1.37/8.50 = 0.16 that displaces the solidus by +120 °C. Melting of the amount 7%/20% for 8.50 mol% H_2O would require temperatures of 776 °C/783 °C, whereas the observed

H_2O content would require 880 °C/1052 °C.

For epidote-biotite GT58, the determined melt volume of ≥3.73% translates to H_2O saturation at 3.94 mol%. With a stoichiometric water content of 2.22 mol%, the equilibrium assemblage has $f_{sat} = 2.22/3.94 = 0.56$. The undersaturation displaces the solidus by +50 °C. Contours of vol.% melt indicate that 7%/20% melt would be produced at 700 °C/868 °C for 3.94 mol% H_2O and 859 °C/914 °C for the stoichiometric content of 2.22 mol%.

6 Discussion

6.1 Melt fertility

We now investigate the roles of hydration and composition on melt potential based on the results of pseudosection analyses of the studied samples. We then consider the implications for the rheology and deformation of mountain belts. Fig. 17 shows the estimated temperatures recorded by our samples (black markers), along with the temperatures required to attain 7 vol.% melt (the 'melt connectivity threshold' of Rosenberg and Handy, 2005) and 20 vol.% melt (the likely lower bound of the 'solid to liquid transition' in terms of the bulk rheology). These temperatures, shown as solid and dashed lines, respectively, are calculated for the stoichiometric water contents (grey) and minimally H_2O saturated contents (red) of the samples. The temperatures were determined at 10 kbar and 8 kbar. Also shown, in red, are the calculated temperatures of the solidus (circles) and the same melt isolines, under the conditions of minimal water saturation at the solidus. Higher water contents than this would not change the solidus temperature, but would reduce the temperatures at which the displayed melt fractions are attained.

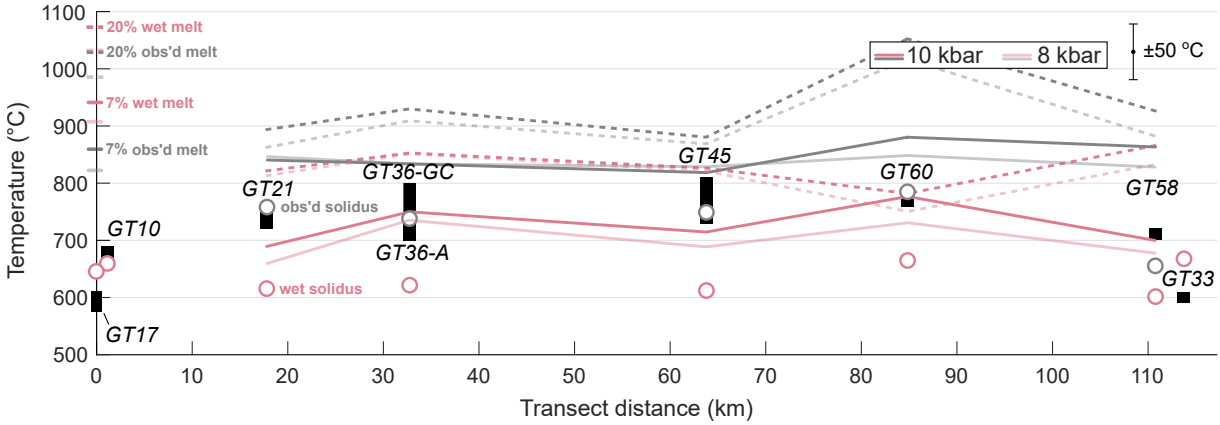


Figure 17: Analysis of sample melting behaviour at 10 kbar. Temperature constraints are shown for sample solidi (circles) and melting (7 vol.% solid lines, 20 vol.% dashed lines) for observed H_2O contents (grey colouring) and at saturation (red colouring). Melt isolines are shown for 10 kbar and 8 kbar. Observed-H_2O melt temperatures are not shown for melanosome sample GT60-M owing to petrographic indicators of melt loss. Of the remaining metasedimentary samples (GT17, GT10, GT33), only GT17 was analysed for melting temperatures.

Psammite GT17 is a noteworthy sample owing to this lithology being the most representative of the metasedimentary portion of the Britt Domain (yellow unit in Fig. 1d; e.g. 'migmatitic biotite gneiss' of Lumbers, 1975). The dominantly quartzo-feldspathic bulk

composition of this sample means that the 7% and 20% melt thresholds calculated are only attained at high temperatures of ≥860 °C at 10 kbar and ≥823 °C at 8 kbar, at the observed water content of 0.8 mol.%, which is above saturation by a factor of 1.6. Thus, a large portion of quartzo-feldspathic rocks across the Britt Domain, with similar chemistry, are unlikely to have undergone significant melting (i.e. ≥7 vol.%) even under conditions of 1.6× oversaturation. Observations of 'melt-like' granitic segregations and layers within these rocks (Lumbers, 1975; Davidson, Culshaw, and Nadeau, 1982; Davidson, 1986; Jamieson et al., 1992; Jamieson, Culshaw, and Corrigan, 1995; Corrigan, Culshaw, and Mortensen, 1994; Wodicka, Ketchum, and Indares, 2000), across the study region and perhaps the Grenville Province as a whole, therefore require an alternative viable explanation.

Overall, the results plotted in Fig. 17 show that H_2O undersaturation has significant effects on melt fertility in chemically diverse rocks as commonly observed in exhumed orogenic mid-crust (Rudnick and Fountain, 1995). At the constrained mid-crustal pressures, temperatures as hot as 800 °C would not have been sufficient for a solid to liquid transition (≥20%; Rosenberg and Handy, 2005) even under H_2O saturation. Although hydrous pelite is an exception to this finding (e.g. migmatite GT60), these lithologies are uncommon as compared to psammite (e.g. sample GT17), which undergo melting of the same degree at >100 °C higher temperatures (Fig. 17).

6.2 Tectonic implications of melt volumes

The tectonic importance of the melt fertility of a mountain belt lies in the influence on the effective viscosity of the ductile crust. Experiments on partially molten rocks have highlighted the rheological effects of melt content, and such melt weakening underpins some dynamic models in which the mid-crust flows as a low-viscosity 'channel' (Beaumont et al., 2004; Godin et al., 2006; Jamieson et al., 2007; Jamieson and Beaumont, 2013). If no melt-enabled weakening occurs, and solid-state mineral creep governs the deformation, then effective viscosities are higher and greater thicknesses of flowing layers are required for deformation at geologically-significant rates (Copley and McKenzie, 2007). Ongoing debates regarding the existence (or otherwise) of rapid flow in thin crustal channels (Beaumont et al., 2004; Royden, 1996), vertically-coupled simple shear of the entire mid- to upper-crust (McKenzie et al., 2000; Copley, Avouac, and Wernicke, 2011), or lateral variations in crustal rheology (Clark and Royden, 2000), are therefore rooted in the melt fertility of the orogenic crust.

Our analysis presented above implies that melt-related weakening is likely to be localised and volumetrically minor in mountain ranges that resemble this area and structural level of the Grenville. The volumetrically-important lithologies are unable to generate significant enough melt volumes at the prevailing P–T conditions to cross the rheological solid-liquid transition, due in part to the water under-saturated nature of the crust. The more fertile lithologies, although being more well-studied because they enable the most accurate P–T determinations to be made, are sufficiently volumetrically-minor that melt weakening is likely to be limited to spatially-disconnected 'pockets' analogous to the seismically-imaged 'bright spots' in the Tibetan crust (Hetenyi et al., 2011; Brown et al., 1996; Basuyau et al., 2013). A prerequisite for rapid flow in melt-weakened mid-crustal channels is therefore likely to be a mountain belt dominated by water-saturated and fertile rocks (e.g. previously-unmetamorphosed mudrocks) that can generate significant melt on large length-scales.

7 Conclusion

The results of combined petrography and P–T pseudosection analyses provide refined constraints on metamorphic conditions across a 130-km across-strike segment of the Canadian Grenville Province, proximal to the Sole Thrust. Peak-metamorphic conditions were ∼10 kbar and ∼750 °C across the two studied thrust sheet (i.e. Britt Domain and Shawanaga Domain).

The results of pseudosection analyses of metamorphic samples across indicate that these rocks lie in a region of metamorphic P–T–$M(H_2O)$ space that straddles the H_2O-undersaturated solidus. Of the eight studied samples, two record low-degree melting (≥5 vol.%; Grt amphibolite GT45 and Ep-Bt amphibolite GT58) and a melt-reintegrated aluminous pelite (GT60) records ≥20 vol.%. The variability in melting broadly correlates with f_{sat} ranging from 0.2 to 0.7 in samples recording metamorphic temperatures of 700–800 °C, in addition to the effects of differing bulk chemistry. Widespread crustal weakening and flow as has previously been proposed (Jamieson et al., 2007; Rivers, 2011; Hynes and Rivers, 2010; Jamieson and Beaumont, 2011) are therefore implausible in this region. Even under conditions of H_2O saturation, metamorphic temperatures in excess of 800 °C (at 10 kbar) would be required to cross the solid-to-liquid transition and achieve bulk crustal weakening and granite formation.

References

Ague, J. (2003). "3.06 - Fluid Flow in the Deep Crust". In: *Treatise on Geochemistry*. Ed. by Heinrich D. Holland and Karl K. Turekian. Oxford: Pergamon, pp. 195–228. ISBN: 978-0-08-043751-4. DOI: 10.1016/B0-08-043751-6/03023-1.

Anovitz, Lawrence M. and E. J. Essene (1990). "Thermobarometry and Pressure-Temperature Paths in the Grenville Province of Ontario". In: *Journal of Petrology* 31.1, pp. 197–241. ISSN: 0022-3530. DOI: 10.1093/petrology/31.1.197.

Argand, Emile (1924). "La Tectonique de l'Asie". In: *Proceedings of the XIIIth International Geological Congress*. Vol. 1. English translation by A. V. Carozzi, The Tectonics of Asia. New York: Hafner Press, 1977, pp. 171–372.

Arzi, Avner A. (1978). "Critical phenomena in the rheology of partially melted rocks". In: *Tectonophysics* 44.1, pp. 173–184. ISSN: 0040-1951. DOI: 10.1016/0040-1951(78)90069-0.

Austrheim, H. (1987). "Eclogitization of lower crustal granulites by fluid migration through shear zones". In: *Earth and Planetary Science Letters* 81.2, pp. 221–232. ISSN: 0012-821X. DOI: https://doi.org/10.1016/0012-821X(87)90158-0.

Avouac, Jean Philippe (2003). "Mountain building, erosion, and the seismic cycle in the Nepal Himalaya". English. In: *Advances in Geophysics* 46.C, pp. 1–80. ISSN: 0065-2687. DOI: 10.1016/S0065-2687(03)46001-9.

Baldwin, J. A. et al. (2005). "Modelling of mineral equilibria in ultrahigh-temperature metamorphic rocks from the Anápolis–Itauçu Complex, central Brazil". In: *Journal of Metamorphic Geology* 23.7, pp. 511–531. ISSN: 0263-4929. DOI: 10.1111/j.1525-1314.2005.00591.x.

Barrow, G. (1912). "On the geology of lower dee-side and the southern highland border". In: *Proceedings of the Geologists' Association* 23.5, 274–IN1. ISSN: 0016-7878. DOI: 10.1016/S0016-7878(12)80018-6.

Basuyau, C. et al. (Apr. 2013). "Joint inversion of teleseismic and GOCE gravity data: application to the Himalayas". In: *Geophysical Journal International* 193.1, pp. 149–160. ISSN: 0956-540X. DOI: 10.1093/gji/ggs110.

Beaumont, C. et al. (2006). "Crustal flow modes in large hot orogens". In: *Channel Flow, Ductile Extrusion and Exhumation in Continental Collision Zones*. Ed. by R. D. Law, M. P. Searle, and L. Godin. Vol. 268. Geological Society London, pp. 91–145. ISBN: 9781862392090. DOI: 10.1144/GSL.SP.2006.268.01.05.

Beaumont, Christopher et al. (2004). "Crustal channel flows: 1. Numerical models with applications to the tectonics of the Himalayan-Tibetan orogen". In: *Journal of Geophysical Research: Solid Earth* 109.B6, pp. 0148–0227. DOI: 10.1029/2003JB002809.

Bégin, N. J. (1992). "Contrasting mineral isograd sequences in metabasites of the Cape Smith Belt, northern Québec, Canada: three new bathograds for mafic rocks". In: *Journal of Metamorphic Geology* 10.5, pp. 685–704. ISSN: 0263-4929. DOI: 10.1111/j.1525-1314.1992.tb00115.x.

Bennett, G., B. O. Dressler, and J. A. Robertson (1991). "The Huronian Supergroup and associated intrusive rocks". In: *Geology of Ontario*. Vol. Special Volume 4, Part 1. Ontario Geological Survey, pp. 549–591.

Berman, Robert G. (1991). "Thermobarometry using multi-equilibrium calculations; a new technique, with petrological applications". In: *The Canadian Mineralogist* 29.4, pp. 833–855. ISSN: 0008-4476.

Bethune, K. M. (1997). "The Sudbury dyke swarm and its bearing on the tectonic development of the Grenville Front, Ontario, Canada". In: *Precambrian Research* 85.3, pp. 117–146. ISSN: 0301-9268. DOI: 10.1016/S0301-9268(96)00052-6.

Bethune, K. M. and A. Davidson (1997). "Grenvillian metamorphism of the Sudbury diabase dyke-swarm; from protolith to two-pyroxene–garnet coronite". In: *The Canadian Mineralogist* 35.5, pp. 1191–1220. ISSN: 0008-4476.

Brown, L. D. et al. (1996). "Bright Spots, Structure, and Magmatism in Southern Tibet from INDEPTH Seismic Reflection Profiling". In: *Science* 274.5293, pp. 1688–1690. DOI: 10.1126/science.274.5293.1688.

Brown, M. (2001). "Crustal melting and granite magmatism: key issues". In: *Physics and Chemistry of the Earth, Part A: Solid Earth and Geodesy* 26.4, pp. 201–212. ISSN: 1464-1895. DOI: 10.1016/S1464-1895(01)00047-3.

– (Apr. 1993). "P–T–t evolution of orogenic belts and the causes of regional metamorphism". In: *Journal of the Geological Society* 150.2, pp. 227–241. ISSN: 0016-7649. DOI: 10.1144/gsjgs.150.2.0227.

Capitani, C. de and K. Petrakakis (2010). "The computation of equilibrium assemblage diagrams with Theriak/Domino software". In: *American Mineralogist* 95, pp. 1006–1016.

Carmichael, D. M. (1969). "On the mechanism of prograde metamorphic reactions in quartz-bearing pelitic rocks". In: *Contributions to Mineralogy and Petrology* 20.3, pp. 244–267. ISSN: 1432-0967. DOI: 10.1007/BF00377479.

Carr, S. D. et al. (2000). "Geologic transect across the Grenville orogen of Ontario and New York". In: *Canadian Journal of Earth Sciences* 37.2-3, pp. 193–216. ISSN: 0008-4077. DOI: 10.1139/e99-074.

Chapman, G. (2017). "Late-stage propagation of the Grenville Orogen: thermobarometry and times of peak metamorphism from Sudbury metadiabase, Georgian Bay, Ontario". Thesis. Dalhousie University.

Clark, Marin Kristen and Leigh Handy Royden (Aug. 2000). "Topographic ooze: Building the eastern margin of Tibet by lower crustal flow". In: *Geology* 28.8, pp. 703–706. ISSN: 0091-7613. DOI: 10.1130/0091-7613(2000)28<703:TOBTEM>2.0.CO;2.

Clemens, J. D. and D. Vielzeuf (1987). "Constraints on melting and magma production in the crust". In: *Earth and Planetary Science Letters* 86.2, pp. 287–306. ISSN: 0012-821X. DOI: 10.1016/0012-821X(87)90227-5.

Coggon, R. and T. J. B. Holland (2002). "Mixing properties of phengitic micas and revised garnet-phengite thermobarometers". In: *Journal of Metamorphic Geology* 20.7, pp. 683–696. ISSN: 0263-4929. DOI: 10.1046/j.1525-1314.2002.00395.x.

Cooper, A. F. (1972). "Progressive Metamorphism of Metabasic Rocks from the Haast Schist Group of Southern New Zealand". In: *Journal of Petrology* 13.3, pp. 457–492. ISSN: 0022-3530. DOI: 10.1093/petrology/13.3.457.

Copley, Alex, Jean-Philippe Avouac, and Brian P. Wernicke (2011). "Evidence for mechanical coupling and strong Indian lower crust beneath southern Tibet". In: *Nature* 472, pp. 79–81. DOI: 10.1038/nature09926.

Copley, Alex and Dan McKenzie (May 2007). "Models of crustal flow in the India-Asia collision zone". In: *Geophysical Journal International* 169.2, pp. 683–698. ISSN: 0956-540X. DOI: 10.1111/j.1365-246X.2007.03343.x.

Corfu, F. and R. M. Easton (2001). "U–Pb evidence for polymetamorphic history of Huronian rocks within the Grenville front tectonic zone east of Sudbury, Ontario, Canada". In: *Chemical Geology* 172.1, pp. 149–171. ISSN: 0009-2541. DOI: 10.1016/S0009-2541(00)00241-2.

Corrigan, D., N. G. Culshaw, and Jim K. Mortensen (1994). "Pre-Grenvillian evolution and Grenvillian overprinting of the Parautochthonous Belt in Key Harbour, Ontario: U–Pb and field constraints". In: *Canadian Journal of Earth Sciences* 31.3, pp. 583–596. ISSN: 0008-4077. DOI: 10.1139/e94-051.

Culshaw, N. G. and Jarda Dostal (1997). "Sand Bay gneiss association, Grenville Province, Ontario: a Grenvillian rift- (and -drift) assemblage stranded in the Central Gneiss Belt?" In: *Precambrian Research* 85.1, pp. 97–113. ISSN: 0301-9268. DOI: 10.1016/S0301-9268(97)00036-3.

Culshaw, N. G., C. C. Gerbi, and J. H. Marsh (2010). "Softening the lower crust: Modes of syn-transport transposition around and adjacent to a deep crustal granulite nappe, Parry Sound domain, Grenville Province, Ontario, Canada". In: *Tectonics* 29.5. ISSN: 0278-7407. DOI: 10.1029/2009TC002537.

Culshaw, N. G. et al. (2013). "Geochemical, geochronological and isotopic constraints on the origin of members of the allochthonous Shawanaga and basal Parry Sound domains, Central Gneiss Belt, Grenville Province, Ontario". In: *Precambrian Research* 228, pp. 131–150. ISSN: 0301-9268. DOI: 10.1016/j.precamres.2013.01.012.

Culshaw, N. G. et al. (2004). *Georgian Bay Geological Synthesis, Grenville Province: Explanatory Notes for Preliminary Maps P.3548 to P.3552*. Open File Report 6143.

Culshaw, N. G. et al. (1988). "Georgian Bay geological synthesis. Key Harbour to Dillon, Grenville Province of Ontario". In: *Current Research, Part C*. Geological Survey of Canada, pp. 129–133.

Culshaw, N. G. et al. (2016). "Kiosk domain, Central Gneiss Belt, Grenville Province, Ontario: A Labradorian palimpsest preserved in the ductile deep crust". In: *Precambrian Research* 280, pp. 249–278. ISSN: 0301-9268. DOI: 10.1016/j.precamres.2016.05.002.

Davidson, A. (1996). *Geology of the Grenville Province (1:2,000,000)*. Report Open file 3346. Geological Survey of Canada.

– (1986). "Grenville Front relationships near Killarney, Ontario". In: *The Grenville Province*. Ed. by J. M. Moore, A. Davidson, and A. J. Baer. Vol. Special Paper 31. Geological Association of Canada, pp. 107–117.

Davidson, A. and K. M. Bethune (1988). "Geology of the north shore of Georgian Bay, Grenville Province of Ontario". In: *Current Research, Part C*. Geological Survey of Canada, Paper 88-1C, pp. 135–144.

Davidson, A., D. M. Carmichael, and D. R. M. Pattison (1990). "Field Trip #1: Metamorphism and geodynamics of the Southwestern Grenville Province, Ontario". In: *International Geological Correlation Program*. Vol. Project 235-304, p. 123.

Davidson, A., N. G. Culshaw, and L. Nadeau (1982). "A Tectono-metamorphic Framework For Part of the Grenville Province, Parry Sound Region, Ontario". In: *Current Research, Part A*. Geological Survey of Canada, pp. 175–190. DOI: 10.4095/111263.

Derry, D. R. (1950). *Tectonic Map of Canada (1:3,801,600)*. Tech. rep. 120 F-1950. Geographical Association of Canada.

Dewey, John F. and Kevin C. A. Burke (1973). "Tibetan, Variscan, and Precambrian Basement Reactivation: Products of Continental Collision". In: *The Journal of Geology* 81.6, pp. 683–692. ISSN: 0022-1376. DOI: 10.1086/627920.

Dyck, Brendan et al. (2020). "Muscovite dehydration melting: Reaction mechanisms, microstructures, and implications for anatexis". In: *Journal of Metamorphic Geology* 38.1, pp. 29–52. ISSN: 0263-4929. DOI: 10.1111/jmg.12511.

Easton, R. M. and E. I. Murphy (2002). *Precambrian Geology of Street Township, Southern and Grenville Provinces*. Report. Ontario Geological Survey.

England, P. C. and A. B. Thompson (1984). "Pressure–Temperature–Time Paths of Regional Metamorphism I. Heat Transfer during the Evolution of Regions of Thickened Continental Crust". In: *Journal of Petrology* 25.4, pp. 894–928. ISSN: 0022-3530. DOI: 10.1093/petrology/25.4.894.

Feng, Peng et al. (2021). "Partial melting of ultrahigh-pressure eclogite by omphacite-breakdown facilitates exhumation of deeply-subducted crust". In: *Earth and Planetary Science Letters* 554, p. 116664. ISSN: 0012-821X. DOI: 10.1016/j.epsl.2020.116664.

Godin, Laurent et al. (2006). "Channel flow, ductile extrusion and exhumation in continental collision zones: an introduction". In: *Channel Flow, Ductile Extrusion and Exhumation in Continental Collision Zones*. Ed. by Robert D. Law, Mike P. Searle, and Laurent Godin. Vol. 268. Geological Society, London, Special Publications. Geological Society of London, pp. 1–23. DOI: 10.1144/GSL.SP.2006.268.01.01.

Green, A. et al. (1988). "Crustal structure of the Grenville front and adjacent terranes". In: *Geology* 16.9, pp. 788–792. ISSN: 0091-7613. DOI: 10.1130/0091-7613(1988)016<0788:CSOTGF>2.3.CO;2.

Green, E. et al. (2016). "Activity-composition relations for the calculation of partial melting equilibria in metabasic rocks". In: *Journal of Metamorphic Geology* 34.9, pp. 845–869. ISSN: 02634929. DOI: 10.1111/jmg.12211.

Hetenyi, G. et al. (2011). "Discontinuous low-velocity zones in southern Tibet question the viability of the channel flow model". In: *Growth and Collapse of the Tibetan Plateau*. Ed. by R. Gloaguen and L. Ratschbacher. Vol. 353. Geological Society of London, pp. 99–108. ISBN: 9781862396012. DOI: 10.1144/SP353.6.

Holland, T. J. B. (2009). *AX: calculate activities of mineral endmembers from chemical analyses*. URL: https://filedn.com/lU1GlyFhv3UuXg5E9dbnWFF/TJBHpages/ax.html.

Holland, T. J. B. and J. Blundy (1994). "Non-ideal interactions in calcic amphiboles and their bearing on amphibole-plagioclase thermometry". In: *Contributions to Mineralogy and Petrology* 116, pp. 433–447. DOI: 10.1007/BF00310910.

Holland, T. J. B. and R. Powell (2011). "An improved and extended internally consistent thermodynamic dataset for phases of petrological interest, involving a new equation of

state for solids". In: *Journal of Metamorphic Geology* 29.3, pp. 333–383. ISSN: 02634929. DOI: 10.1111/j.1525-1314.2010.00923.x.
Holness, Marian B. and E. W. Sawyer (2008). "On the Pseudomorphing of Melt-filled Pores During the Crystallization of Migmatites". In: *Journal of Petrology* 49.7, pp. 1343–1363. ISSN: 0022-3530. DOI: 10.1093/petrology/egn028.
Hynes, A. and T. Rivers (2010). "Protracted continental collision — evidence from the Grenville OrogenThis article is one of a series of papers published in this Special Issue on the theme Lithoprobe — parameters, processes, and the evolution of a continent". In: *Canadian Journal of Earth Sciences* 47.5, pp. 591–620. ISSN: 0008-4077. DOI: 10.1139/E10-003.
Indares, A. (2020). "Deciphering the metamorphic architecture and magmatic patterns of large hot orogens: Insights from the central Grenville Province". In: *Gondwana Research* 80, pp. 385–409. ISSN: 1342-937X. DOI: 10.1016/j.gr.2019.10.013.
– (2024). "The Grenville Province: revisiting the orogenic framework and integrating recent findings". In: *Canadian Journal of Earth Sciences* 62.2, pp. 99–118. ISSN: 0008-4077. DOI: 10.1139/cjes-2023-0143.
Jamieson, R. A. and C. Beaumont (2011). "Coeval thrusting and extension during lower crustal ductile flow – implications for exhumation of high-grade metamorphic rocks". In: *Journal of Metamorphic Geology* 29.1, pp. 33–51. ISSN: 0263-4929. DOI: 10.1111/j.1525-1314.2010.00908.x.
– (2013). "On the origin of orogens". In: *GSA Bulletin* 125.11-12, pp. 1671–1702. ISSN: 0016-7606. DOI: 10.1130/B30855.1.
Jamieson, R. A., N. G. Culshaw, and D. Corrigan (1995). "North-west propagation of the Grenville orogen: Grenvillian structure and metamorphism near Key Harbour, Georgian Bay, Ontario, Canada". In: *Journal of Metamorphic Geology* 13.2, pp. 185–207. ISSN: 0263-4929. DOI: 10.1111/j.1525-1314.1995.tb00213.x.
Jamieson, R. A. et al. (2007). "Synconvergent ductile flow in variable-strength continental crust: Numerical models with application to the western Grenville orogen". In: *Tectonics* 26.5. ISSN: 0278-7407. DOI: 10.1029/2006TC002036.
Jamieson, R. A. et al. (1992). "Timing and tectonic setting of Grenvillian metamorphism—constraints from a transect along Georgian Bay, Ontario". In: *Journal of Metamorphic Geology* 10.3, pp. 321–332. ISSN: 0263-4929. DOI: 10.1111/j.1525-1314.1992.tb00087.x.
Johnson, T. E., R. White, and R. Powell (2008). "Partial melting of metagreywacke: a calculated mineral equilibria study". In: *Journal of Metamorphic Geology* 26.8, pp. 837–853. ISSN: 0263-4929. DOI: 10.1111/j.1525-1314.2008.00790.x.
Ketchum, J. W. F. et al. (1994). "1.45 Ga granulites in the southwestern Grenville province: Geologic setting, P-T conditions, and U-Pb geochronology". In: *Geology* 22.3, pp. 215–218. ISSN: 0091-7613. DOI: 10.1130/0091-7613(1994)022<0215:GGITSG>2.3.CO;2.
Ketchum, J. W. F. et al. (1998). "Timing and thermal influence of late orogenic extension in the lower crust: a UPb geochronological study from the southwest Grenville orogen, Canada". In: *Precambrian Research* 89.1, pp. 25–45. ISSN: 0301-9268. DOI: 10.1016/S0301-9268(97)00079-X.
Kohn, M. J. (2014). "Himalayan Metamorphism and Its Tectonic Implications". In: 42.Volume 42, 2014, pp. 381–419. ISSN: 1545-4495. DOI: 10.1146/annurev-earth-060313-055005.
Kohn, Matthew J., Sean P. Long, and T. Mark Harrison (2024). "Himalayan leucogranites; a minimal role in deformation". In: *Elements* 20.6, pp. 381–387. ISSN: 1811-5209. DOI: 10.2138/gselements.20.6.381.

Krogh, T. E. (1994). "Precise U-Pb ages for Grenvillian and pre-Grenvillian thrusting of Proterozoic and Archean metamorphic assemblages in the Grenville Front tectonic zone, Canada". In: *Tectonics* 13.4, pp. 963–982. ISSN: 0278-7407. DOI: 10.1029/94TC00801.

Kwak, T. A. P. (1971). "Justification for Both Ionic and Thermal Reactions in Grenville Province Pelitic Rocks near Sudbury, Ontario, Canada". In: *Canadian Journal of Earth Sciences* 8.11, pp. 1333–1354. ISSN: 0008-4077. DOI: 10.1139/e71-124.

Le Fort, P. et al. (1987). "Crustal generation of the Himalayan leucogranites". In: *Tectonophysics* 134.1, pp. 39–57. ISSN: 0040-1951. DOI: 10.1016/0040-1951(87)90248-4.

Li, Xiaoyan et al. (2020). "Calculating biotite formula from electron microprobe analysis data using a machine learning method based on principal components regression". In: *Lithos* 356-357, p. 105371. ISSN: 0024-4937. DOI: 10.1016/j.lithos.2020.105371.

Lumbers, S. B. (1975). *Geology of the Burwash Area, Districts of Nipissing, Parry Sound, and Sudbury; Accompanied by Map 2271, scale 1 inch to 2 miles*. Report GR116. Ontario Division of Mines.

Maruyama, S., J. G. Liou, and K. Suzuki (1982). "The peristerite gap in low-grade metamorphic rocks". In: *Contributions to Mineralogy and Petrology* 81.4, pp. 268–276. ISSN: 1432-0967. DOI: 10.1007/BF00371681.

McKenzie, D. (1970). "Plate Tectonics of the Mediterranean Region". In: *Nature* 226.5242, pp. 239–243. DOI: 10.1038/226239a0.

McKenzie, Dan et al. (2000). "Characteristics and consequences of flow in the lower crust". In: *Journal of Geophysical Research: Solid Earth* 105.B5, pp. 11029–11046. DOI: 10.1029/1999JB900446.

McLellan, Eileen (1985). "Metamorphic Reactions in the Kyanite and Sillimanite Zones of the Barrovian Type Area". In: *Journal of Petrology* 26.4, pp. 789–818. ISSN: 0022-3530. DOI: 10.1093/petrology/26.4.789.

Mehnert, K. R. (1968). *Migmatites and the origin of granitic rocks, by K. R. Mehnert*. Amsterdam, New York [etc.: Amsterdam, New York [etc.] Elsevier Pub. Co., 1968.

Molina, J. F. et al. (2015). "Calcic amphibole thermobarometry in metamorphic and igneous rocks: New calibrations based on plagioclase/amphibole Al-Si partitioning and amphibole/liquid Mg partitioning". In: *Lithos* 232, pp. 286–305. ISSN: 0024-4937. DOI: 10.1016/j.lithos.2015.06.027.

Molnar, Peter and Hélène Lyon-Caen (1988). "Some simple physical aspects of the support, structure, and evolution of mountain belts". In: *Processes in Continental Rifting*. Ed. by K. L. Kleinspehn and C. Paola. Vol. 218. GSA Special Papers. Geological Society of America, pp. 179–207. DOI: 10.1130/SPE218-p179.

Molnar, Peter and Paul Tapponnier (1975). "Cenozoic Tectonics of Asia: Effects of a Continental Collision". In: *Science* 189.4201, pp. 419–426. DOI: 10.1126/science.189.4201.419.

Murphy, E. I. (1999). "Geology, metamorphism, and geochemistry of Southern and Grenville Province rocks in the vicinity of the Grenville Front, Timmins Creek area, near Sudbury, Ontario". Thesis. Laurentian University.

Nicoli, G. and B. Dyck (2018). "Exploring the metamorphic consequences of secular change in the siliciclastic compositions of continental margins". In: *Geoscience Frontiers* 9.4, pp. 967–975. ISSN: 1674-9871. DOI: 10.1016/j.gsf.2017.12.009.

Ontario Geological Survey (2011). *1:250 000 Scale Bedrock Geology of Ontario*.

– (1974). *Burwash (Map 2271): Nipissing, Parry Sound and Sudbury Districts*. Ontario Geological Survey.

Palin, R. M. et al. (2016). "High-grade metamorphism and partial melting of basic and intermediate rocks". In: *Journal of Metamorphic Geology* 34.9, pp. 871–892. ISSN: 0263-4929. DOI: 10.1111/jmg.12212.

Pryer, L. L. (1985). *Preliminary Report on the Grenville Front Tectonic Zone, Carlyle Township, Ontario*. Vol. Ontario Geological Survey Paper 85-1A, pp. 463–483.

Rivers, T. (2008). "Assembly and preservation of lower, mid, and upper orogenic crust in the Grenville Province—Implications for the evolution of large hot long-duration orogens". In: *Precambrian Research* 167.3, pp. 237–259. ISSN: 0301-9268. DOI: 10.1016/j.precamres.2008.08.005.

– (1997). "Lithotectonic elements of the Grenville Province: review and tectonic implications". In: *Precambrian Research* 86.3, pp. 117–154. ISSN: 0301-9268. DOI: 10.1016/S0301-9268(97)00038-7.

– (2011). "Upper-crustal orogenic lid and mid-crustal core complexes: signature of a collapsed orogenic plateau in the hinterland of the Grenville Province; This article is one of a series of papers published in CJES Special Issue: In honour of Ward Neale on the theme of Appalachian and Grenvillian geology". In: *Canadian Journal of Earth Sciences* 49.1, pp. 1–42. ISSN: 0008-4077. DOI: 10.1139/e11-014.

Rivers, T. et al. (1989). "New tectonic divisions of the Grenville Province, Southeast Canadian Shield". In: *Tectonics* 8.1, pp. 63–84. ISSN: 0278-7407. DOI: 10.1029/TC008i001p00063.

Rivers, T. et al. (2012). "The Grenville Orogen - A post-LITHOPROBE perspective". In: *Tectonic Styles in Canada*. Ed. by K. A. Percival, F. A. Cook, and R. M. Clowes. Vol. 49. Geological Association of Canada. Chap. 3, pp. 97–236.

Rosenberg, C. L. and M. R. Handy (2005). "Experimental deformation of partially melted granite revisited: implications for the continental crust". In: *Journal of Metamorphic Geology* 23.1, pp. 19–28. ISSN: 0263-4929. DOI: 10.1111/j.1525-1314.2005.00555.x.

Royden, Leigh (1996). "Coupling and decoupling of crust and mantle in convergent orogens: Implications for strain partitioning in the crust". In: *Journal of Geophysical Research: Solid Earth* 101.B8, pp. 17679–17705. DOI: 10.1029/96JB00951.

Rudnick, Roberta L. and David M. Fountain (1995). "Nature and composition of the continental crust: A lower crustal perspective". In: *Reviews of Geophysics* 33.3, pp. 267–309. ISSN: 8755-1209. DOI: 10.1029/95RG01302.

Sawyer, E. W. (2008). *Atlas of Migmatites*. Canadian Science Publishing. ISBN: 9780660197876. DOI: 10.1139/9780660197876.

– (2001). "Melt segregation in the continental crust: distribution and movement of melt in anatectic rocks". In: *Journal of Metamorphic Geology* 19.3, pp. 291–309. ISSN: 0263-4929. DOI: 10.1046/j.0263-4929.2000.00312.x.

Slagstad, T. et al. (2024). "Complementarity of Hf isotopes from detrital and igneous zircon: an example from the Central Gneiss Belt, Grenville Province, Ontario". In: *Canadian Journal of Earth Sciences* 62.2, pp. 192–210. ISSN: 0008-4077. DOI: 10.1139/cjes-2024-0017.

Slagstad, T. et al. (2004). "Timing and duration of melting in the mid orogenic crust: Constraints from U–Pb (SHRIMP) data, Muskoka and Shawanaga domains, Grenville Province, Ontario". In: *Canadian Journal of Earth Sciences* 41.11, pp. 1339–1365. ISSN: 0008-4077. DOI: 10.1139/e04-068.

Spear, Frank S., Matthew J. Kohn, and John T. Cheney (1999). "P-T paths from anatectic pelites". In: *Contributions to Mineralogy and Petrology* 134.1, pp. 17–32. ISSN: 1432-0967. DOI: 10.1007/s004100050466. URL: https://doi.org/10.1007/s004100050466.

Tafur, Lorena A. and Johann F. A. Diener (2020). "Mineral equilibrium constraints on the feasibility of diffusive H2O-fluxed melting in the continental crust". In: *Journal of Metamorphic Geology* 38.7, pp. 719–742. ISSN: 0263-4929. DOI: 10.1111/jmg.12536.

Thompson, A. B. (1983). "Fluid-absent metamorphism". In: *Journal of the Geological Society* 140.4, pp. 533–547. DOI: 10.1144/gsjgs.140.4.0533.

Torvela, Taija and Matti Kurhila (2020). "How does orogenic crust deform? Evidence of crustal-scale competent behaviour within the partially molten middle crust during orogenic compression". In: *Precambrian Research* 342, p. 105670. ISSN: 0301-9268. DOI: 10.1016/j.precamres.2020.105670.

Tuccillo, M. E. et al. (1992). "Thermobarometry, Geochronology and the Interpretation of P–T–t Data in the Britt Domain, Ontario Grenville Orogen, Canada". In: *Journal of Petrology* 33.6, pp. 1225–1259. ISSN: 0022-3530. DOI: 10.1093/petrology/33.6.1225.

Van Breemen, O. et al. (1986). "U–Pb zircon geochronology of Grenville tectonites, granulites and igneous precursors, Parry Sound, Ontario". In: *The Grenville Province*. Ed. by J. M. Moore, A. Davidson, and A. J. Baer. Vol. 31. Special Paper. Geological Association of Canada, pp. 191–207.

Volante, Silvia et al. (2025). "Oxygen isotope shifts reveal fluid-fluxed melting in continental anatexis". In: *Communications Earth Environment* 6.1, p. 282. ISSN: 2662-4435. DOI: 10.1038/s43247-025-02250-z. URL: https://doi.org/10.1038/s43247-025-02250-z.

Weinberg, Roberto F., E. Veveakis, and K. Regenauer-Lieb (June 2015). "Compaction-driven melt segregation in migmatites". In: *Geology* 43.6, pp. 471–474. ISSN: 0091-7613. DOI: 10.1130/G36562.1. eprint: https://pubs.geoscienceworld.org/gsa/geology/article-pdf/43/6/471/3547315/471.pdf.

Weller, O. M. et al. (2021). "The metamorphic and magmatic record of collisional orogens". In: *Nature Reviews Earth and Environment* 2.11, pp. 781–799. ISSN: 2662-138X. DOI: 10.1038/s43017-021-00218-z.

White, D. et al. (2000). "A seismic-based cross-section of the Grenville Orogen in southern Ontario and western Quebec". In: *Canadian Journal of Earth Sciences* 37.2-3, pp. 183–192. ISSN: 0008-4077. DOI: 10.1139/e99-094.

White, R. et al. (2014). "New mineral activity–composition relations for thermodynamic calculations in metapelitic systems". In: *Journal of Metamorphic Geology* 32.3, pp. 261–286. ISSN: 0263-4929. DOI: 10.1111/jmg.12071.

White, R. W., R. Powell, and T. J. B. Holland (2007). "Progress relating to calculation of partial melting equilibria for metapelites". In: *Journal of Metamorphic Geology* 25.5, pp. 511–527. ISSN: 0263-4929. DOI: 10.1111/j.1525-1314.2007.00711.x.

Whitney, D. L. and B. W. Evans (2010). "Abbreviations for names of rock-forming minerals". In: *American Mineralogist* 95.185-187. DOI: 10.2138/am.2010.3371.

Whyte, A. J. et al. (2021). "Quantifying Water Diffusivity and Metamorphic Reaction Rates Within Mountain Belts, and Their Implications for the Rheology of Cratons". In: *Geochemistry, Geophysics, Geosystems* 22.11, e2021GC009988. DOI: 10.1029/2021GC009988.

Wodicka, N., J. W. F. Ketchum, and R. Indares (2000). "Grenvillian metamorphism of monocyclic rocks, Georgian Bay, Ontario, Canada: implications for convergence history". In: *The Canadian Mineralogist* 38.2, pp. 471–510. ISSN: 0008-4476. DOI: 10.2113/gscanmin.38.2.471.

Wynne-Ewards, H. R. (1972). "The Grenville Province, Variations in Tectonic Styles in Canada". In: *Special Paper of the Geological Association of Canada* 11, pp. 263–334.